KTH ROYAL INSTITUTE
OF TECHNOLOGY

Degree Project in Physics

Second cycle 30 credits

Improving tau decay simulations for detecting tau neutrinos at IceCube

SIMON THOR

Stockholm, Sweden 2024

Physics

Improving tau decay simulations for detecting tau neutrinos at IceCube

Simon Thor
simtho@kth.se
SH204X Degree Project in Engineering Physics, Second Cycle
Department of Physics
Royal Institute of Technology (KTH)

Supervisors: Jason Koskinen, Chad Finley, and Christian Ohm
Examiner: Jonas Strandberg

June 4, 2024

Abstract

The tau neutrino is one of the least understood elementary particles, as it is difficult to detect. One of the few detectors that can detect it is the IceCube neutrino observatory, located on the south pole. When a tau neutrino interacts with an atomic nucleus in the ice at IceCube, a tau lepton can form, which then decays almost instantaneously. The decay products of the tau lepton will then emit light, which can be detected at IceCube. To gain a better understanding of tau neutrinos, it is therefore crucial to accurately simulate tau lepton decays.

In this thesis, simulated tau decays in the IceCube simulation framework are evaluated and compared to tau decay simulations in TAUOLA, a high-precision tau decay simulation library. Through this work, several issues with the current simulations were discovered. Specifically, the polarization of the tau lepton is neglected, hadronic resonances are not implemented for tau decays, and several decay modes are missing. These issues result in an overestimate of the energy of the visible decay products, which means that the light emitted from the tau decay is dimmer in reality than what is predicted by the current IceCube simulations. To address this, TAUOLA was integrated into the IceCube simulations, thereby enabling high-precision tau decay simulations for future studies.

Sammanfattning

Tauneutrinon är en av de allra minst studerade elementarpartiklarna på grund av att den är svår att detektera. En av få detektorer som han observera tauneutriner är neutrinoteleskopet IceCube vid sydpolen. När en tauneutrino interagerar med isen kan en taulepton skapas, som snabbt sönderfaller. De partiklar som bildas vid sönderfallet avger ljus som kan mätas i IceCube. För att kunna studera tauneutriner är det därför fundamentalt att simulera korrekta och noggranna tausönderfall.

I detta examensarbete jämfördes IceCubes simuleringar av tausönderfall med simuleringar av tausönderfall i TAUOLA, ett mjukvarubibliotek ämnat för högprecisionssimuleringar av tausönderfall. Genom detta upptäcktes ett flertal problem med IceCubes simuleringar: ingen hänsyn tas till polariseringen av tauleptonen, hadroniska resonanser är inte implementerade, och det finns ett flertal sätt som tauleptonen kan sönderfalla på som inte är implementerade. Dessa problem leder till att energin hos de observerbara partiklarna som produceras vid sönderfallet överskattas, vilket innebär att ljuset som avges i verkligheten är mindre än vad simuleringarna förutspår. För att lösa dessa problem integrerades TAUOLA i IceCubes simuleringsramverk, vilket möjliggör precisa tausönderfallssimuleringar för framtida analyser inom IceCube.

Contents

Chapter 1

Introduction

The goal of particle physics is to better understand the smallest building blocks of the universe. Strangely, the smallest objects are deeply connected to the universe as a whole, as the evolution and fate of the universe highly depends on how the fundamental particles interact with each other. Understanding the properties of these building blocks and how they interact with each other is therefore crucial for answering some of humanity's most fundamental questions, such as how the universe began, what everything around us is made out of, and how the universe will end.

There are still many unanswered questions within particle physics, and many of them are believed to be linked to neutrinos: some of the most elusive particles in the universe. In particular, the tau neutrino is one of the least understood elementary particles, as it is particularly difficult to measure. Currently, the only way of measuring tau neutrinos and distinguishing them from other neutrino interactions is if they interact with matter and produce tau leptons. However, due to the large mass of the tau lepton, only high-energy tau neutrinos can produce tau leptons. Furthermore, the tau lepton will quickly decay, making it difficult to determine if a tau lepton was produced or not.

The topic of this thesis is precisely to investigate the decays of tau leptons produced by tau neutrinos. Understanding how the tau leptons decay and how much of the tau energy is transferred to each decay product is crucial to better understand the tau neutrino.

The outline of the thesis is as follows. First, background material relevant for this study is presented in Chapter 2, including additional details about neutrinos, tau leptons, the IceCube neutrino observatory, and tau neutrino detection at IceCube. In Chapter 3, the aim of this thesis, and the method and software used in this study is presented. In Chapter 4, the results from this study are presented and analyzed. Finally, in Chapter 5, the connection between the different results, as well as their implications for tau neutrino searches at IceCube are presented. The thesis is also summarized in Chapter 5.

Chapter 2

Background

2.1 Neutrinos

Neutrinos are some of the least understood particles in the Standard Model (SM). This is because the neutrinos only interact via the weak force and gravity, and as such, interactions between neutrinos and other particles are rare, making them difficult to observe. Furthermore, the weak force only acts on (anti-)particles with left(right)-handed chirality. Since neutrinos have only be detected through the weak force, only left-handed neutrinos have ever been detected and are the only types of neutrinos included in the Standard Model. This means that neutrinos are massless according to the Standard Model, as the right-handed counterpart of a particle is required for the neutrino to have mass through the Higgs mechanism. However, many experiments have shown that neutrinos have mass, by detecting neutrino oscillations [1].

2.1.1 Neutrino oscillations

In the Standard Model, there are three neutrino flavors: electron neutrino, muon neutrino and tau neutrino, which are the electromagnetically neutral counterparts to the changed electron, muon and tau leptons. In addition to this, there are three neutrino mass eigenstates, which are described by the equation

$$\mathcal{H} \left|\nu_k\right\rangle = E_k \left|\nu_k\right\rangle , \tag{2.1}$$

where $\mathcal{H}$ is the hamiltonian operator, $E_k = \sqrt{p^2 + m_k^2}$ is the k:th energy eigenvalue with p and m_k denoting the neutrino three-momentum and mass respectively, and $\left|\nu_k\right\rangle$ is the k:th neutrino energy eigenfunction, with a mass m_k [1]. Note that natural units are used throughout this thesis, where $\hbar = c = 1$.

The time evolution of the mass state is described by the Schrödinger equation, which gives

$$\left|\nu_k(t)\right\rangle = e^{-iE_k t} \left|\nu_k\right\rangle , \tag{2.2}$$

where $\left|\nu_k\right\rangle = \left|\nu_k(t=0)\right\rangle$ for some arbitrary starting time [1]. Both the flavor and mass eigenstates span the same space that describe the neutrinos, but act as different basis vectors. As such, there are three mass eigenstates $k \in \{1, 2, 3\}$ (since there are three

flavor states) and we can transform from one basis to the other. This is done through the Pontecorvo-Maki-Nakagawa-Sakata (PMNS) matrix, and the relation between these states is then given by

$$\text{Convert massive state to flavor state: } |\nu_\alpha(t)\rangle = \sum_k U^*_{\alpha k} e^{-iE_k t} |\nu_k\rangle \,, \tag{2.3}$$

$$\text{Convert flavor state to massive state: } |\nu_k\rangle = \sum_\alpha U_{\alpha k} |\nu_\alpha\rangle \,, \tag{2.4}$$

where $U_{\alpha k}$ is the PMNS matrix, which is a unitary matrix [1], and $\alpha \in \{e, \mu, \tau\}$ describes the flavor. Combining equations 2.3 and 2.4, we can describe the time evolution of the flavor state as

$$|\nu_\alpha(t)\rangle = \sum_{\beta=e,\mu,\tau} \left(\sum_k U^*_{\alpha k} e^{-iE_k t} U_{\beta k} \right) |\nu_\beta\rangle \,. \tag{2.5}$$

This shows that, as long as U is not the identity matrix, a neutrino traveling through space will switch between different flavors, and the transition probability from a flavor α to another flavor β is given by

$$\underset{\nu_\alpha \to \nu_\beta}{P}(t) = |\langle \nu_\beta \mid \nu_\alpha(t) \rangle|^2 = \sum_{k,j} U^*_{\alpha k} U_{\beta k} U_{\alpha j} U^*_{\beta j} e^{-i(E_k - E_j)t}, \tag{2.6}$$

where k, j are indices for all possible neutrino mass eigenstates [1].

For one neutrino traveling through space, the neutrino momentum will be constant and the only difference between different energy eigenstates will be the neutrino mass. Additionally, since the neutrino is so light ($m < 1$ eV [2]), the energy of the neutrino is dominated by its momentum. Using this one can rewrite the energy of neutrinos by utilizing Taylor expansion

$$E_k = \sqrt{p^2 + m_k^2} \approx E + \frac{m_k^2}{2E} \tag{2.7}$$

$$\implies E_k - E_j \approx \frac{m_k^2 - m_j^2}{2E} = \frac{\Delta m^2_{kj}}{2E} \tag{2.8}$$

where $\Delta m^2_{kj} \equiv m_k^2 - m_j^2$. Finally, since the neutrino energy is dominated by its momentum, the velocity is approximately the speed of light, which in natural units gives $L \approx t$ where L is the distance traveled by the neutrino [1].

This can then be used to rewrite the transition probability as

$$\underset{\nu_\alpha \to \nu_\beta}{P}(L) = \sum_{k,j} U^*_{\alpha k} U_{\beta k} U_{\alpha j} U^*_{\beta j} e^{-i\frac{\Delta m^2_{kj} L}{2E}}. \tag{2.9}$$

2.1.2 Neutrino interactions

There are two ways in which neutrinos can interact with other particles: neutral current (NC) and charged current (CC) interactions [3].

NC interactions are when a Z boson is exchanged between the particles in the interaction, and is called neutral current since the Z boson is electrically neutral. An example of such an interaction is shown in Figure 2.1, where the neutrino is scattered off of a neutron. Typically, in neutrino experiments such as IceCube, this happens when the neutrino scatters off of a nucleon inside a nucleus.

CC interactions are when a W boson is exchanged between the particles interacting, and is called charged current since the W boson is electrically charged. When a neutrino is scattered off of a particle via a CC interaction, the neutrino is converted into a charged lepton. This charged lepton always has the same flavor as the neutrino, i.e. if the interaction neutrino is an electron neutrino, the outgoing lepton is an electron and similarly for muon and tau neutrinos. The main focus of this thesis is CC interactions and specifically CC tau neutrino interactions, which is what is shown in Figure 2.1.

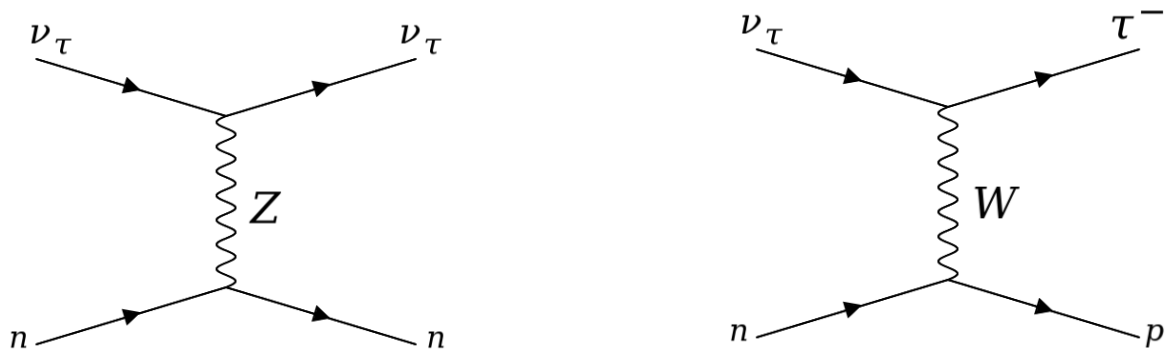

Figure 2.1: Feynman diagram examples of neutrino interactions. The cases shown here are for a tau neutrino interacting with a neutron. The left diagram shows a NC interaction, while the right diagram shows a CC interaction.

2.2 The IceCube experiment

IceCube, situated at the South Pole, is a neutrino observatory that uses the Antarctic ice as a detector. In a volume of approximately 1 km^3 of ice, 5160 Digital Optical Modules (DOMs) distributed across 86 vertical strings have been drilled in. DOMs are downward-facing photo-multiplier tubes that are highly sensitive to photons. The vertical distance between DOMs on the same string is roughly 17 m, and the horizontal distance between strings is approximately 125 m [3, 4]. A schematic of the IceCube observatory is shown in Figure 2.2.

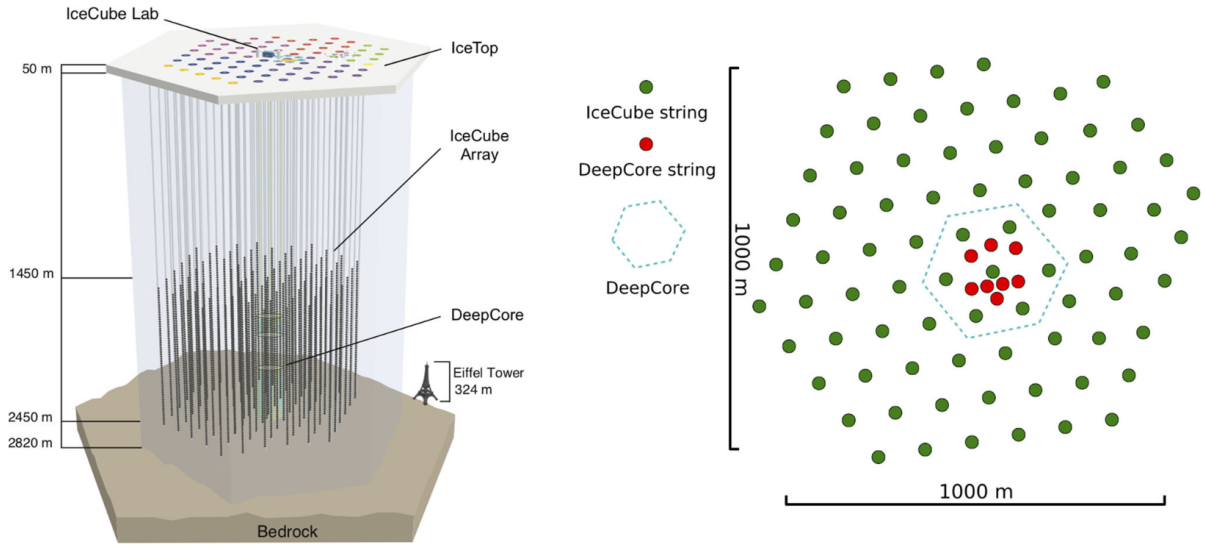

Figure 2.2: Schematic of the IceCube neutrino observatory. Figure obtained from [5].

IceCube is a unique neutrino detector, not only due to its location, but also its physics discovery potential. With is unrivaled volume, it can detect rare ultra high-energy neutrinos. IceCube is the leading project in trying to uncover the sources of these ultra high-energy neutrinos, with results so far suggesting that the neutrinos originate from cataclysmic astrophysical events and objects such as active galactic nuclei [6].

When neutrinos from cosmic rays and astrophysical sources such as galaxies reach IceCube, they sometimes interact with the ice. The charged particles created in this interaction will travel faster than the speed of light in ice and emit a cone of light, similar to the phenomenon of a sonic boom. This light is called Cherenkov radiation, and is detected by the DOMs in the ice. Based on the amount of light and the timing that different DOMs detect the light, the direction and energy of the original neutrino can be reconstructed [3].

For neutral current interactions, most of the light is emitted close to the neutrino-nucleus interaction point, with the light coming from the shower of hadrons created from the nucleus. For charged current interactions with electron neutrinos, in addition to the hadronic cascade, the electron produced will also create a shower that generates Cherenkov radiation. These types of events are known as cascade-like event [3]. For the case of a CC interaction with a muon neutrino, a shower of hadrons is again created from the nucleus. In addition to this, the muon, due to its long lifetime, will travel through the ice a long distance, emitting Cherenkov radiation along its path. This is known as a track-like event [3].

Tau neutrino interactions can appear as both cascade-like and track-like events, depending on the decay mode. For tau neutrinos and tau charged current interactions, if the tau lepton decays to a muon, the event will be track-like, while if the tau lepton decays hadronically or to an electron, the event will be cascade-like [3, 4]. Schematics of both track-like and cascade-like events are shown in Figure 2.3.

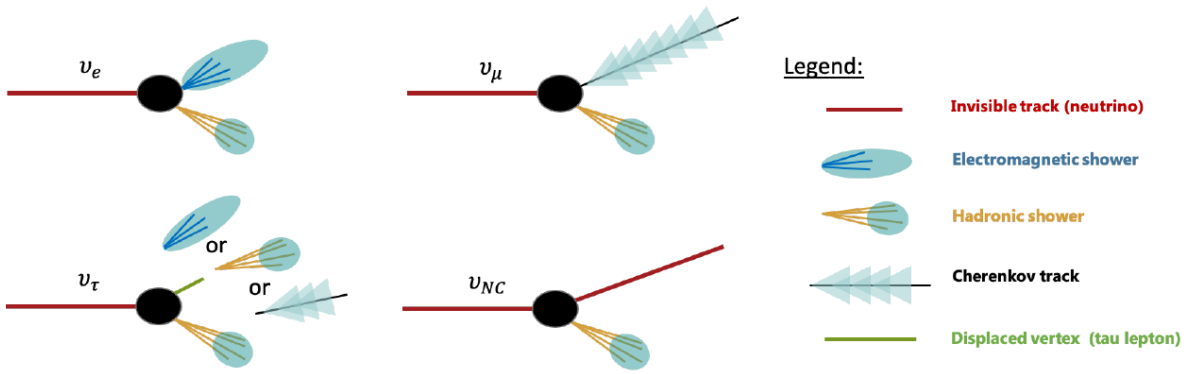

Figure 2.3: Schematics of the different ways that neutrinos can interact with nuclei in IceCube. The top left schematic shows an electron neutrino, which results in a cascade-like event. The top right schematic shows a muon neutrino interaction, which typically results in a track-like event. The bottom left shows the tau neutrino, where the tau lepton can either decay to a muon (track-like), electron (cascade-like) or hadrons (cascade-like). The bottom right image shows a NC interaction, which results in a cascade-like event. Image from Ref. [3].

2.2.1 Tau neutrino appearance searches at IceCube

Close to the center of IceCube, the density of DOMs is higher, making it more sensitive to neutrinos of lower energies ($\mathcal{O}(10)$ GeV compared to the rest of IceCube which is only sensitive to neutrinos with energies $\gtrsim 100$ GeV). This part is known as IceCube DeepCore and can be used to study low-energy atmospheric neutrinos [4].

The atmospheric neutrinos can be utilized for neutrino oscillation studies and specifically tau neutrino appearance searches. Due to the large mass of the tau lepton, there are a negligible number of tau leptons being produced in the atmosphere. Instead, the main source of tau neutrinos detected at IceCube is muon neutrinos that have oscillated and become tau neutrinos. For the muon neutrino energy range of $\mathcal{O}(1-100)$ GeV, the probability of a muon neutrino oscillating into a tau neutrino is large if it travels a distance roughly equivalent to the diameter of the Earth (as governed by the relation between L and E in Equation (2.9)).

Since tau leptons mostly (roughly 65% of the time) decay hadronically, which results in a cascade, one expects to see an excess in cascade-like events when muon neutrinos, which otherwise would have resulted in track-like events, become tau neutrinos.

The combination of the large volume of IceCube DeepCore, the energy ranges of neutrinos that can be detected, and the ability to distinguish track-like from cascade-like events makes IceCube one of few experiments that is able to measure muon neutrinos oscillating into tau neutrinos. The most recent search for tau neutrinos at IceCube was Ref. [4], and a new search is currently in progress, with improved simulations and more data. For the most recent study, the events that were used in the analysis had a reconstructed energy (that is, the visible energy that is detected through light in the IceCube DeepCore detector) of $5.6-56$ GeV [4]. In Ref. [4], several different cuts were applied to remove background events, mainly atmospheric muons. Monte Carlo (MC)

simulations of oscillating atmospheric neutrinos were performed, where the interactions with the ice, the propagation of the light through the ice, detector effects, and the same reconstruction and cuts were applied. The reconstructed energy, direction, and particle ID (i.e. if it is a track-like or cascade-like event) was then calculated for each event (both MC and data), and the events were then binned into a 3D histogram (projected onto its three axes) with regards to these three parameters. The histogram of MC samples was then compared to the histogram of measured events. From this comparison, it is then possible to determine if tau neutrinos have been detected or not. An example of this kind of 3D histogram, from Ref. [4], is shown in Figure 2.4.

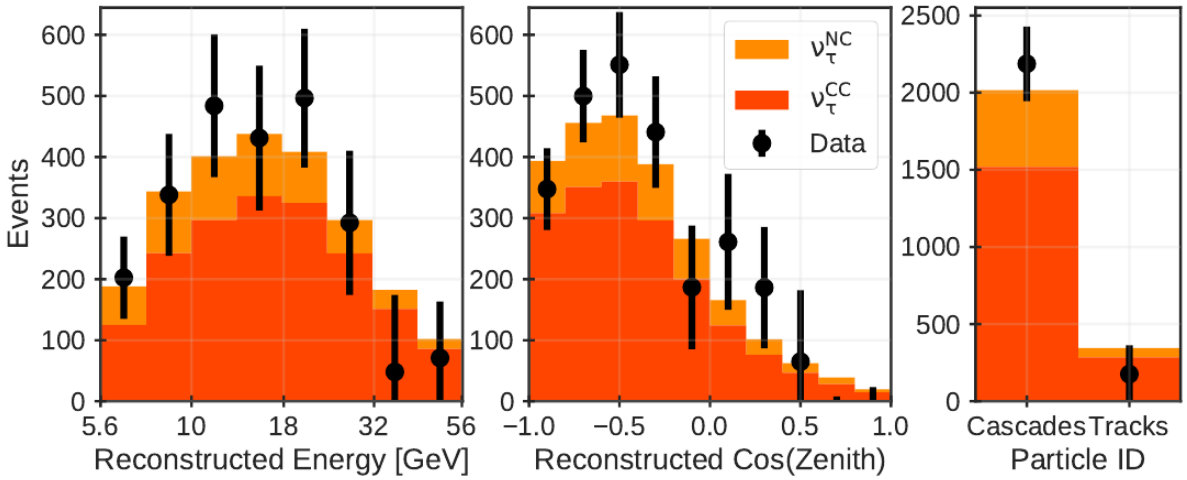

Figure 2.4: The distribution of the expected vs observed number of tau neutrinos, from the most recent atmospheric tau neutrino appearance search by IceCube [4]. Since tau neutrinos cannot be identified on an event-by-event basis, the "Data" distributions shown here are the data distributions of all events with the expected background of muons and neutrinos subtracted. In reality, the distribution of events is a 3D distribution, with the parameters particle ID (track-like or cascade-like), reconstructed energy, and reconstructed cos(zenith angle) of the incoming neutrino. What is shown here is the projection of the 3D histogram on the three axes.

The histogram of the MC samples depend on so-called nuisance parameters. These include the mixing angle between the muon and tau neutrino, the squared mass difference between the muon and tau neutrino, and more. After all cuts are applied, a scan over the space of these nuisance parameters is performed to find the parameter combination that gives the best fit between the data and the MC histograms. One of the nuisance parameters is the tau neutrino normalization, which effectively scales the histogram up or down. If the normalization is 1, no scaling is applied, and if normalization is 0.5, the tau neutrino histogram is scaled to be half as large as it originally was. The best-fit tau neutrino normalization value was found to be 0.75 for this study, i.e. more fewer tau neutrino events were detected than expected from MC simulations. The deviation from 1 is however less than one standard deviation [4].

2.3 Tau decays

For tau neutrino CC interactions, the reconstructed neutrino energy and direction is based on the visible decay products (i.e. non-neutrino decay products) of the tau lepton that is produced. The tau lepton itself is never observed directly for atmospheric neutrino, where the energy is typically < 100 GeV, as the tau lepton only has a lifetime of $t_\tau \approx 2.90 \cdot 10^{-13}$ seconds [7, 2]. With a tau mass of $m_\tau \approx 1.777$ GeV, a 100 GeV tau lepton would only travel an average distance of $t_\tau c\sqrt{(E/m_\tau)^2 - 1} \approx 5$ mm before decaying, which is much smaller than the meter-scale resolution of IceCube. Simulating the tau decays accurately is therefore fundamental for tau neutrino appearance searches, to be able to correctly reconstruct the incoming tau neutrino. The main tau decay modes are summarized in Table 2.1. In the following sections, details regarding the tau decay that affect the energy and direction of the tau lepton decay products are described.

Decay mode	$\mathcal{BR}$ [%]
$\pi^-\nu_\tau$	11.1
$\mu^-\overline{\nu}_\mu\nu_\tau$	17.1
$e^-\overline{\nu}_e\nu_\tau$	15.2
$\pi^-\pi^0\nu_\tau$	25.3
$\pi^-\pi^0\pi^0\nu_\tau$	9.2
$\pi^-\pi^-\pi^+\nu_\tau$	8.9
$\pi^-\pi^-\pi^+\pi^0\nu_\tau$	4.6
$e^-\overline{\nu}_e\gamma\nu_\tau$	2.9
Other	5.8

Table 2.1: The largest tau decay modes. The first column shows the decay products of the tau, the second column shows the branching ratio of the decay mode (in %, calculated empirically from roughly 70 000 simulated tau decay events with TAUOLA).

2.3.1 Hadronic resonances

Almost always, hadronic tau decays that are not two-body decays ($\tau^- \to \pi^-\nu_\tau, \tau^- \to K^-\nu_\tau$) go via a resonance, where a massive meson and a neutrino are created, after which the meson quickly decays to several lighter mesons. The dominant resonances are $\tau^- \to \rho(770)\nu_\tau^- \to \pi^-\pi^0\nu_\tau$, $\tau^- \to a_1(1260)\nu_\tau^- \to \pi^-\pi^0\pi^0\nu_\tau$, and $\tau^- \to a_1(1260)\nu_\tau^- \to \pi^-\pi^-\pi^+\nu_\tau$ [7, 8]. Here, the ρ and a_1 mesons have the same composition as pions ($u\overline{d}, \overline{u}d, (u\overline{u} - d\overline{d})/\sqrt{2}$) but are heavier, have spin 1 and slightly different quantum numbers [9]. Examples of resonance decays are shown in Figure 2.5.

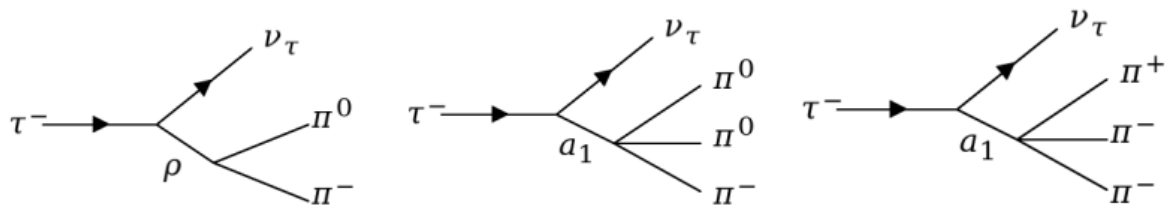

Figure 2.5: Examples of hadronic tau decays through the resonance mesons ρ and a_1. The decays shown here are the ones that dominate the hadronic tau decays.

2.3.2 Polarization

The polarization (also known as helicity) is a vector $\vec{P} = [P_x.P_y, P_z]^T$ that describes the spin vector relative to the tau momentum vector. A polarization vector pointing in the same direction as the momentum is called right-handed, while the polarization being anti-parallel to the momentum is known as left-handed. For energies where the produced tau lepton energy is much greater than m_τ, the polarization becomes the same as the chirality. This means that if the tau lepton is produced through the weak interaction, and the produced tau has a high energy, the polarization will typically be left-handed, since the weak force only acts on particles with left-handed chirality.

The polarization of the tau lepton affects in which direction the decay products are emitted in. This is because both the spin and the four-momentum must be conserved during the decay. For example, consider the decay mode $\tau^- \to \pi^-\nu_\tau$ for a left-handed tau lepton. The tau lepton and tau neutrino have spin 1/2, while π^- has spin 0, and the tau neutrino is always left-handed due to its close-to-zero (zero in SM) mass, and since it is always produced through the weak interaction. In the rest frame of the left-handed tau lepton, to conserve the spin, the neutrino tends to move in the opposite direction as the tau lepton spin, which in the lab frame is in the same direction as the tau. To conserve momentum, the pion must then move in the same direction as the tau spin, i.e. anti-parallel to the tau lepton momentum in the lab frame. Thus, the polarization has affected the direction of the decay products, and the same principle is applicable to all other decay modes. This pion decay mode example is also explained visually in Figure 2.6.

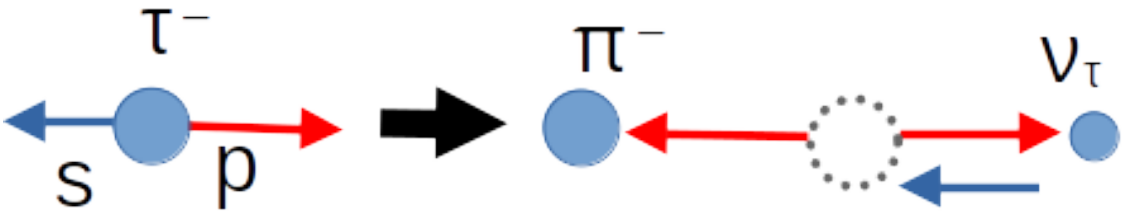

Figure 2.6: Schematic of the $\tau^- \to \pi^- \nu_\tau$ decay for a left-handed tau lepton. The figure shows the rest frame, where the red arrow shows the momentum direction, the blue arrows show the spin directions, the left figure shows before the decay, and the right figure shows are the decay.

2.4 Tau polarization in neutrino-nucleus scattering

For neutrino-nucleus interactions, the spin vector always lies in the neutrino-tau momentum plane according to the Standard Model. One can therefore describe the polarization vector with only two components by changing the coordinate system. The two components of the polarization vector are the longitudinal component P_L, which is in the tau momentum direction, and P_T which is the transverse component, and is orthogonal to the tau momentum direction but still in the tau-neutrino plane. Here, the transverse direction is defined as $(\vec{k} \times \vec{k}') \times \vec{k}'/|(\vec{k} \times \vec{k}') \times \vec{k}'|$, where $\vec{k}$ is the incoming neutrino momentum and $\vec{k}'$ is the outgoing tau momentum [10].

In this case, the magnitude of the longitudinal polarization component is defined as

$$P_L \equiv \frac{\sigma_R - \sigma_L}{\sigma_R + \sigma_L}, \tag{2.10}$$

where σ_R and σ_L are the cross sections for producing a lepton where the spin is pointing in the momentum direction (i.e. right-handed) and the opposite direction (i.e. left-handed), respectively [11]. A particle is unpolarized if $\mathcal{P} \equiv \sqrt{P_L^2 + P_T^2} = 0$, and fully polarized if $\mathcal{P} = 1$. The polarization components can also be rewritten as $P_T = P \sin\theta_P, P_L = P \cos\theta_P$, where P is the magnitude of the polarization vector and the angle θ_P describes the angle between the polarization vector and the tau momentum vector.

The polarization vector depends on the incoming neutrino four-momentum k, the incoming nucleon four-momentum p with mass M, and the outgoing tau four-momentum k' with mass m_τ. Certain interaction types can also depend on other values relevant to their interactions, but this will be discussed in further detail in later sections. We first define some relevant kinematic variables. The momentum transfer is defined as $q \equiv k - k'$, while $Q^2 \equiv -q^2$ is the magnitude of the momentum transfer, $W = \sqrt{(p+q)^2}$ is the hadronic invariant mass, and the Björken $x = Q^2/(2p \cdot q)$ which can be interpreted as the fraction of energy that is passed to the nucleon [12]. Note that the $(+---)$ convention is used in this thesis. Assuming a stationary nucleon, i.e., $p = [M, 0, 0, 0]$, and a neutrino moving in the positive z direction, i.e., $k = [E_\nu, 0, 0, E_\nu]$, the polarization vector is given

by (from Ref. [12])

$$P_L = \mp\frac{1}{2}\left\{\left(2W_1 - \frac{m_\tau^2}{M^2}W_4\right)(p_\tau - E_\tau\cos\theta) + W_2\,(p_\tau + E_\tau\cos\theta)\right. \tag{2.11}$$
$$\left. \pm\,\frac{W_3}{M}\left((E_\nu + E_\tau)\,p_\tau - \left(E_\nu E_\tau + p_\tau^2\right)\cos\theta\right) - \frac{m_\tau^2}{M}W_5\cos\theta\right\}/F$$

$$P_T = \mp\frac{m_\tau\sin\theta}{2}\left(2W_1 - W_2 \pm \frac{E_\nu}{M}W_3 - \frac{m_\tau^2}{M^2}W_4 + \frac{E_\tau}{M}W_5\right)/F \tag{2.12}$$

$$F = \left(2W_1 + \frac{m_\tau^2}{M^2}W_4\right)(E_\tau - p_\tau\cos\theta) + W_2\,(E_\tau + p_\tau\cos\theta) \tag{2.13}$$
$$\pm\,\frac{W_3}{M}\left(E_\nu E_\tau + p_\tau^2 - (E_\nu + E_\tau)\,p_\tau\cos\theta\right) - \frac{m_\tau^2}{M}W_5.$$

Here, $W_n, n \in \{1,2,3,4,5\}$ are the structure functions (not to be confused with the hadronic invariant mass W). These structure functions depend on the neutrino-nucleus interaction type. The three major interaction types are quasi-elastic (QEL), resonance (RES), and deep inelastic scattering (DIS), which are illustrated in Figure 2.9 and described in further detail below. When $\pm$ or $\mp$ is written in the equations above, the top sign corresponds to a τ^-, while the bottom sign corresponds to τ^+. The formulas are taken from Ref. [12] and [13], but are included here for completion. For derivations of the formulas, see Refs. [11, 12, 13]. An example of the tau polarization for neutrino-nucleus interactions, calculated using the formula above, is shown in Figure 2.7.

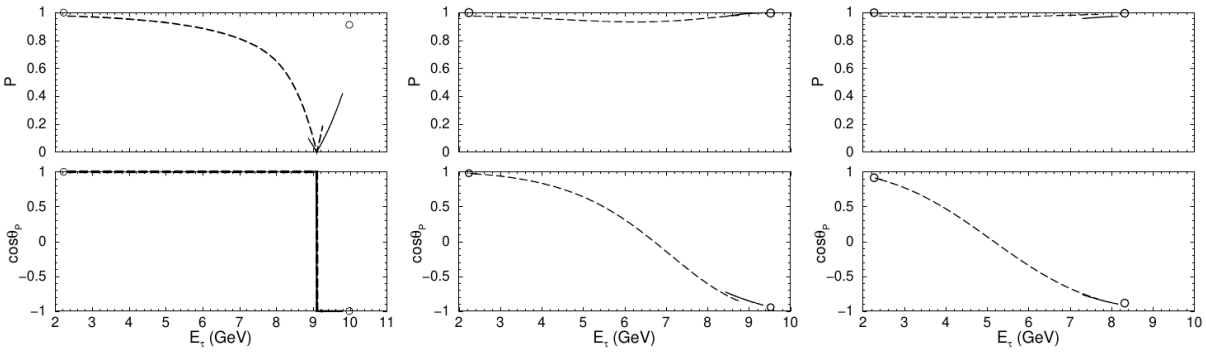

Figure 2.7: The theoretical polarization as a function of the outgoing tau energy and its angle. The polarization depends on the interaction type, and these are therefore shown as separate lines, where the circles are QEL events, dashed lines are DIS events, and full lines are RES events. Note that since QEL events are almost elastic, only two tau energies are physically allowed for each tau outgoing angle. The first row shows the polarization magnitude, while the second row shows the angle of the polarization vector $\cos\theta_P$. Each column correspond to different angles of the outgoing tau lepton relative to the incoming neutrino. The left column shows an angle of 0°, the center column shows 5°, and the right column shows 10°. The figure is from Ref. [12].

While the formula above assumes a stationary nucleon, this is in general not true, unless the nucleus only consists of one nucleon. There are different models describing

the nucleon motion, but the one used in the simulations in this thesis is the relativistic Fermi gas (RFG) model [14, 15], where the nucleon momentum distribution is shown in Figure 2.8.

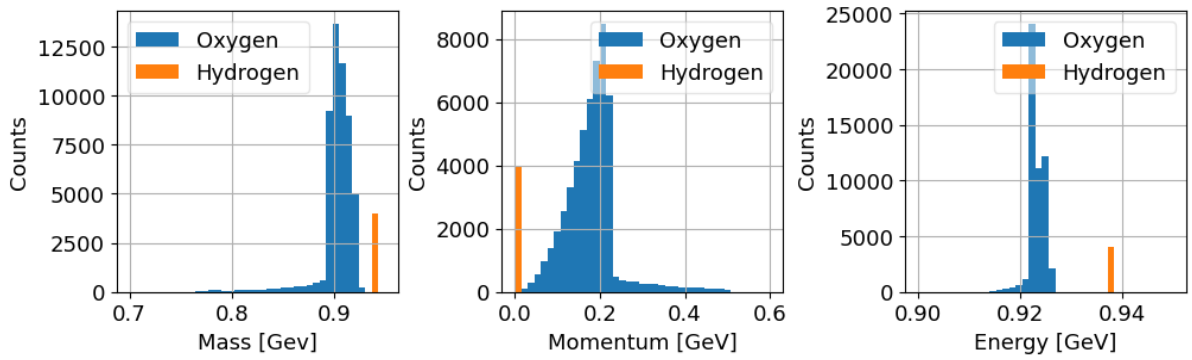

Figure 2.8: The distributions of the nucleon mass (left), momentum (center), and energy (right) according to the relativistic Fermi gas model, which is used in the simulations of this study. The different colors indicate if the hit nucleon is an oxygen atom or a hydrogen atom. The distribution contains 42493 simulated nucleons.

To work around this problem, a coordinate transformation can be applied such that Equations 2.11-2.13 become valid. We first begin with the general four-momenta of the nucleon $p = [E_n, p_{xn}, p_{yn}, p_{zn}]$ and neutrino $k = [E_\nu, k_x, k_y, k_z]$. First the system is boosted to the rest frame of the nucleon, such that p becomes $p_1 = [M, 0, 0, 0]$. We now have $k_1 = [E_{1\nu}, k_{1x}, k_{1y}, k_{1z}]$. To fix the neutrino momentum, we rotate the coordinates such that the neutrino is moving in the $+z$ direction. We then have the same nucleon momentum p_1, while the neutrino momentum becomes $k_2 = [E_{2\nu}, 0, 0, E_{2\nu}]$. By doing this, the criteria for the formulas are fulfilled. Since the structure functions and the tau polarization formulas only depend on dot products between four-vectors (e.g., Björken x, W, and Q^2), which are Lorenz invariant, the reference frame and rotation of the system does not affect the polarization. These transformations of the coordinate system will therefore have no physical effect.

In the following sections, the structure functions and tau polarization calculations are described in more detail for each interaction type.

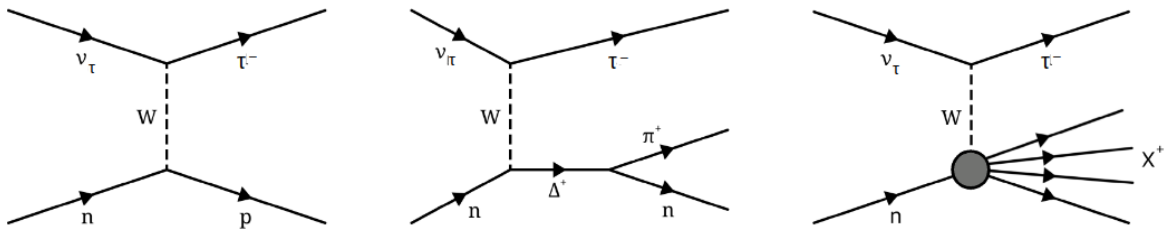

Figure 2.9: Feynman diagrams of QEL (left), RES (center) and DIS (right) neutrino-nucleus interactions. The figure is a modified version from Ref. [3].

2.4.1 Quasi-elastic scattering

Quasi-elastic scattering (QEL) is when the neutrino scatters off of a nucleon and changes a proton into a neutron, or vice versa. A Feynman diagram of this is shown in Figure 2.9. For this interaction, the structure functions are given by (from Ref. [13])

$$W_n = \cos^2(\theta_C) w^{-1} \omega_n(q^2) \delta(1-x) \tag{2.14}$$

$$\omega_1 = |F_A|^2 + x' \left(|F_A|^2 + |F_V + F_M|^2 \right), \tag{2.15}$$

$$\omega_2 = |F_V|^2 + |F_A|^2 + x' \left(|F_M|^2 + 4 |F_T|^2 \right), \tag{2.16}$$

$$\omega_3 = -2\mathcal{R}\mathbf{e} \left[F_A^* \left(F_V + F_M \right) \right], \tag{2.17}$$

$$\omega_4 = \mathcal{R}\mathbf{e} \left[F_V^* \left(F_S - \frac{1}{2} F_M \right) - F_A^* \left(F_T + F_P \right) \right] + x' \left(\frac{1}{2} |F_M - F_S|^2 + |F_T + F_P|^2 \right) \tag{2.18}$$

$$- \frac{1}{4} (1 + x') |F_M|^2 + \left(1 + \frac{1}{2} x' \right) |F_S|^2,$$

$$\omega_5 = 2\mathcal{R}\mathbf{e} \left[F_S^* \left(F_V - x' F_M \right) - F_T^* \left(F_A - 2x' F_P \right) \right] + \omega_2 \tag{2.19}$$

where $x' \equiv -q^2/(4M^2)$, and $\delta(1-x)$ is a δ-function that forces the Björken x to be 1. In reality, this is however not the case for the simulations used in this thesis. This δ-function is therefore dropped in practice. $\mathcal{R}\mathbf{e}$ only selects the real part, and * means that the conjugate value is taken. However, since all functions used here are real, in practice they do not have any effect on the outcome.

The form factors that appear in the ω terms above are (from Ref. [12])

$$F_V = \frac{G_E^V(q^2) - \frac{q^2}{4M^2} G_M^V(q^2)}{1 - \frac{q^2}{4M^2}} \tag{2.20}$$

$$G_E^V = \frac{1}{\left(1 - \frac{q^2}{M_V^2} \right)^2} \tag{2.21}$$

$$F_M = \frac{1}{\xi} \frac{G_M^V(q^2) - G_E^V(q^2)}{1 - \frac{q^2}{4M^2}} \tag{2.22}$$

$$G_M^V = \frac{1+\xi}{\left(1 - \frac{q^2}{M_V^2} \right)^2} \tag{2.23}$$

$$F_S = 0 \tag{2.24}$$

$$F_A = \frac{F_A(0)}{\left(1 - \frac{q^2}{M_A^2} \right)^2} \tag{2.25}$$

$$F_T = 0 \tag{2.26}$$

$$F_p = 2M^2 \frac{F_A(q^2)}{m_\pi^2 - q^2}, \tag{2.27}$$

where $M_V = 0.84$ GeV, $\xi = 3.706$ is the difference between the proton and neutron

anomalous magnetic moments, $M_A = 1.0$ GeV, $F_A(0) = -1.23$, $m_\pi = 0.139$ GeV is the pion mass [12].

2.4.2 Resonance scattering

Resonance scattering (RES) is when the neutrino scatters off of a nucleon and in the process, the nucleon is excited into a more energetic state. This state is known as a hadronic resonance, and will quickly decay into several more stable particles, resulting in a hadronic shower (see Figure 2.9). If the neutrino interacts with a proton, the hadronic resonance is typically a Δ^{++} baryon, and if it interacts with a neutron, it is typically a Δ^{+} baryon, though this depends on the incoming neutrino energy. Note that Δ^{++} consists of uuu, where the spins of all quarks are aligned, while Δ^{+} consists of uud (i.e. same as a proton) with the spins of all quarks being aligned.

For RES, the polarization formula in Equations 2.11 - 2.13 were not used. Instead, an updated formula was used, based on the Berger-Sehgal model for resonance scattering [16], which in turn builds upon the Rein-Sehgal model for cross section calculations for RES neutrino-nucleus interactions [17]. In the Berger-Sehgal model, the polarization vector is given by

$$P_T = \frac{\Sigma_{++} - \Sigma_{--}}{\Sigma_{++} + \Sigma_{--}} \tag{2.28}$$

$$P_L = \frac{\Sigma_{+-} + \Sigma_{-+}}{\Sigma_{++} + \Sigma_{--}} \tag{2.29}$$

$$\Sigma_{\lambda\lambda'} = \sum_{i=L,R,S} c_i^{\lambda} c_i^{\lambda'} \sigma_i^{\lambda\lambda'} \tag{2.30}$$

where c_i^{λ} are coefficients that depend on the charged leptonic currents j_λ in the rest frame of the resonance, and $\sigma_i^{\lambda\lambda'}$ are partial cross sections [18]. Here, $i \in \{L, R, S\}$ is the helicity of the resonance particle. The partial cross sections are given by (from Ref. [18])

$$\sigma_{L,R}^{\lambda\lambda'} = \frac{\pi W}{2M} \left(A_{\pm 3}^{\lambda} A_{\pm 3}^{\lambda'} + A_{\pm 1}^{\lambda} A_{\pm 1}^{\lambda'} \right) \tag{2.31}$$

$$\sigma_{S}^{\lambda\lambda'} = \frac{\pi M |\mathbf{q}|^2}{2WQ^2} \left(A_{0+}^{\lambda} A_{0+}^{\lambda'} + A_{0-}^{\lambda} A_{0-}^{\lambda'} \right), \tag{2.32}$$

where $A_j^{\lambda}, j \in \{-3, -1, 0+, 0-, +1, +3\}$ are known as helicity amplitudes and have different forms depending on the resonance that is produced (i.e. if it is a Δ^{++} or some other particle). Both the helicity amplitudes A_j^{λ} and coefficients c_i^{λ} are calculated in the simulation software automatically for resonance events. To calculate the polarization for RES events, it is therefore only necessary to extract these values from the simulation software.

2.4.3 Deep inelastic scattering

In deep inelastic scattering, the neutrino interacts with an individual quark inside the nucleon, and the nucleon is destroyed and creates a shower of hadrons in the process. An

example interaction is shown in Figure 2.9. For neutrino interactions at IceCube, this is the dominating interaction type.

In addition to the three four-momentum vectors, for DIS, the polarization vector also depends on which quark is produced in the interaction. The structure functions are given by (from Ref. [12])

$$W_1 = \left(1 + \frac{\xi M^2}{p \cdot q}\right) F_1\left(x, Q^2\right) \tag{2.33}$$

$$W_{i=2,\ldots,5} = \frac{M^2}{p \cdot q} F_{i=2,\ldots,5}\left(x, Q^2\right) \tag{2.34}$$

where p, q, M, x and Q^2 are described earlier. The variable ξ is similar to x but corrections have been applied to account for the outgoing quark. If the outgoing quark is a charm quark, $\xi = x(Q^2 + m_c^2)/Q^2$. For all other outgoing quarks, $\xi = x$. The form factors $F_i(x, Q^2)$ depend on the parton distribution functions (PDFs) of the nucleons. PDFs are semi-empirical distributions describing the contents of a nucleon and the probability density of interacting with a certain quark inside a nucleon, as a function of x and Q^2.

The PDF set used in the neutrino-nucleus interaction simulations is the Bodek-Yang corrected GRV98LO PDF set. For consistency, the same PDF set with the same correction is therefore used for the polarization calculation. The so-called Bodek-Yang slightly changes to form factors that are calculated from the PDFs to make them valid for low Q^2 values. Without this correction, the GRV98LO PDF set otherwise is only valid for $Q^2 > 0.8$ GeV^2 [19]. Additionally, only the leading order the PDF set is used (as indicated by the "LO" in the PDF name) as the higher order corrections are not valid for low Q^2 values.

As an example, the GRV98LO PDFs for $Q^2 = 5$ GeV^2 are shown in Figure 2.10. Note that since the GRV98LO PDFs are mainly suited for low-energy interactions ($\lesssim 1$ TeV neutrinos), the PDF values for the heavy (c, b, t) quarks are always set to 0.

As a cross-check, the same tau polarization calculations were done using the C10nlo [20] PDF set without Bodek-Yang corrections, which is commonly used in e.g., LHC analyses. While not shown here, the deviation in the polarization values between the C10nlo and Bodek-Yang corrected GRV98LO PDF sets are relatively small for the neutrino and tau energies that are investigated in this study, with the largest deviations being present for low-energy incoming neutrinos.

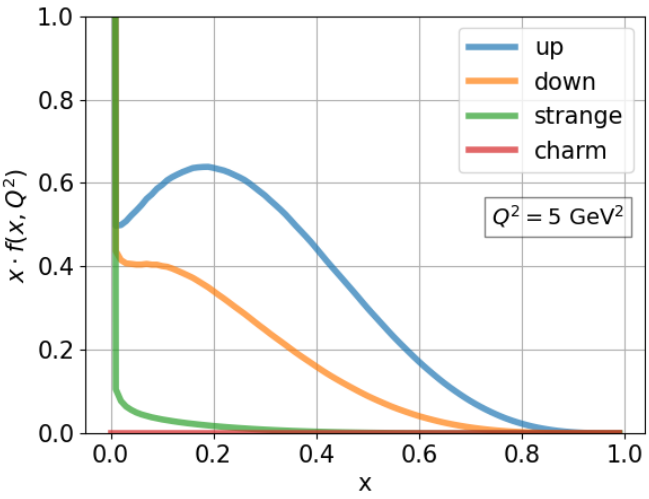

Figure 2.10: The GRV98LO PDF for a proton times the Björken x, as a function of the Björken x. Here, $Q^2 = 5$ GeV^2.

2.4.4 Other interaction types

A small fraction of the simulated events are coherent scattering (COH) events. These are events where the neutrino interacts with the entire nucleus, rather than with just one nucleon or quark [21, 22]. However, for all the simulations of tau neutrinos in this study, less than 0.1% of the events were coherent scattering events. The effects of these events are therefore assumed to be negligible, and tau leptons produced through coherent scattering are assumed to be unpolarized.

Chapter 3

Method

3.1 Software

In this section, the programming languages and software libraries used for this study are listed.

The IceCube simulation framework consists of multiple software libraries that handle various parts of the simulation chain when a neutrino interacts with the ice. First, a neutrino is generated and the interaction with a nucleus, either an oxygen or hydrogen nucleus in the ice, is simulated using GENIE [23, 21, 24], which is built upon PYTHIA6 [25] and ROOT [26]. The particles that are produced in this interaction, i.e., the nucleus remnants and the outgoing lepton (a neutrino for NC interactions and a charged lepton for CC interactions), are then passed to Geant4 [27, 28, 29]. In Geant4, the particles are propagated and absorbed in the ice. The decays of unstable particles, such as the tau lepton, are also simulated in Geant4. After this, simulations of the light emitted from these particles and its absorption by DOMs are also performed in Geant4. While Geant4 is accurate in simulating the propagation of particles in ice, it can be slow for high-energy particles, as they propagate far through the ice and emit large quantities of light and secondary particles. If the outgoing particles are above a certain energy threshold, they are therefore passed to PROPOSAL [30] instead of Geant4, which can perform faster (but slightly less accurate) particle propagation and decay simulations.

In addition to the libraries in the IceCube simulation framework, there are several software packages that are used in this study. TAUOLA [31] is a library specifically developed for high-precision τ decay simulations, and is used by most of the high-precision tau analyses [32, 33, 34]. TAUOLA can simulate τ decays with an arbitrary polarization vector that can either be defined in the lab frame or in the tau rest frame, supports hadronic resonance decays, and most tau decay modes.

PYTHIA8 is another library that will be used in this study. It is often used for simulating high-energy collisions between subatomic particles, such as proton-proton collisions in the LHC [35]. However, it can also be used as a pure τ decay simulator [36]. The implementation is not as extensive as TAUOLA, as there is only support for setting the P_L component of the polarization, with P_T always being 0. Note that only PYTHIA8 has polarization support for τ decays, while PYTHIA6, i.e. the version used in GENIE, does

not.

Analyzing and visualizing the data for this study was done in `Python` using `NumPy` [37], `Pandas` [38, 39], `pyhepmc` [40, 41], `vector` [42] and `matplotlib` [43].

3.2 Problem formulation

For tau neutrino appearance searches, it is fundamental to accurately simulate tau decays, since the incoming tau neutrino will be reconstructed based on the energy and direction of the visible decay products of the tau lepton. If the current tau decay simulations were inaccurate in some way, this would result in an unphysical discrepancy between simulation and data. This could then significantly affect the results of tau neutrino appearance searches, as well as other tau neutrino searches, such as searches for astrophysical tau neutrinos [44].

The goal of this study is to investigate the accuracy of the tau decay simulations in the IceCube simulation framework. This is done by simulating tau neutrino interactions and tau decays in IceCube, as well as simulating polarized tau decays using TAUOLA, which we assume to be the most accurate tau decay simulations. Various distributions of parameters related to the tau lepton decay products are analyzed and compared between Geant4, PROPOSAL, TAUOLA and PYTHIA8. Possible discrepancies between these and their potential impacts on tau neutrino appearance searches are discussed.

3.3 Method

First, 100 000 mono-energetic neutrinos interacting with ice are simulated using GENIE, for energies of 5, 10, 20, 50, and 100 GeV (i.e. 500 000 events in total). From these, only the CC interactions are extracted and the decay products from Geant4 are stored. In Table 3.1, the number of events that are CC, QEL, RES, DIS, and COH are shown for each neutrino energy.

Neutrino energy [GeV]	5	10	20	50	100
All events	100 000	100 000	100 000	100 000	100 000
CC	17881	42493	56282	66363	70092
QEL	9682	7006	3396	1166	474
RES	8199	14101	7303	2633	1184
DIS	0	21386	45583	62488	68379
COH	0	0	0	76	55

Table 3.1: The number of simulated events for each neutrino energy (columns) and the different interaction types (rows). Note that the QEL, RES, DIS and COH counts add up to be the same as the CC count.

Using these events, validation of TAUOLA is first performed. This is done by simulating decays of the tau leptons produced by GENIE. The polarization is either set to be unpolarized or fully polarized, and distributions of various parameters are then compared

to theoretically calculated distributions. Based on these results, the accuracy of TAUOLA is evaluated. Cross-checks are also performed with tau decays using PYTHIA8.

Once the outputs of TAUOLA have been validated, the polarization vectors of the tau leptons are calculated. The polarization is calculated based on the procedure and formulas given in Section 2.4. This polarization vector, in combination with the tau lepton four-momentum, is passed to TAUOLA to simulate the decays. The TAUOLA tau decays are then compared to the Geant4 tau decays. The differences and similarities are evaluated and discussed for the different tau decay modes and parameter distributions. TAUOLA decays with fully left-handed polarization and unpolarized TAUOLA decays are also simulated and used for comparisons. While no simulations of tau decays with PROPOSAL are performed, energy distributions from Ref [8] are compared to equivalent TAUOLA distributions, in order to evaluate potential issues with PROPOSAL.

Lastly, potential solutions for improving tau decay simulations within IceCube are investigated and implemented into the IceCube simulation framework.

The full source code for the analysis in this thesis is available in a repository on Github [45].

Chapter 4

Results

4.1 Validation of TAUOLA

Before investigating the differences between TAUOLA and Geant4, it is crucial to make sure that the TAUOLA decays are accurate and the outputs match the theoretical distributions. In Ref. [11], several theoretically calculated distributions are given for various tau decay modes and decay products, which are compared to the simulated TAUOLA distributions. Note that all histograms shown in the Results section are, unless specified explicitly, normalized such that the integral of the histogram is 1. Furthermore, the error bars are the 1σ Poisson errors.

First, the decay mode $\tau^- \to \pi^- \nu_\tau$ is investigated. In the tau rest frame, it is expected that the π^- angle relative to the tau follows the distribution (given in Ref. [11])

$$\frac{1}{\Gamma_\tau}\frac{\mathrm{d}\Gamma_\pi}{\mathrm{d}\cos\theta} = B_\pi \frac{1}{2}\left(1 + P_L \cos\theta\right), \tag{4.1}$$

where B_π is the branching ratio of $\tau^- \to \pi^- \nu_\tau$, P_L is the longitudinal polarization component, and θ is the angle between π^- and the tau in the tau rest frame [11]. The distributions for the fully polarized left-handed case ($P_L = -1$) and unpolarized ($P_L = 0$) TAUOLA decays are shown in Figure 4.1, along with the theoretical distributions.

We see an almost perfect agreement between theory and the TAUOLA output. The distributions also make intuitive sense, since the π^- has spin 0 while the ν_τ has spin 1/2. For spin to be conserved in the fully polarized case, the ν_τ must move in the same direction as the tau, and for momentum to be conserved, the π^- must move in the opposite direction. In other words, an angle of $\cos\theta = -1$ is favored for the π^-. For the unpolarized case, there is no correlation between the tau spin direction and the momentum direction. As such, the pion distribution should be uncorrelated with the tau momentum direction, which is precisely what we see in Figure 4.1.

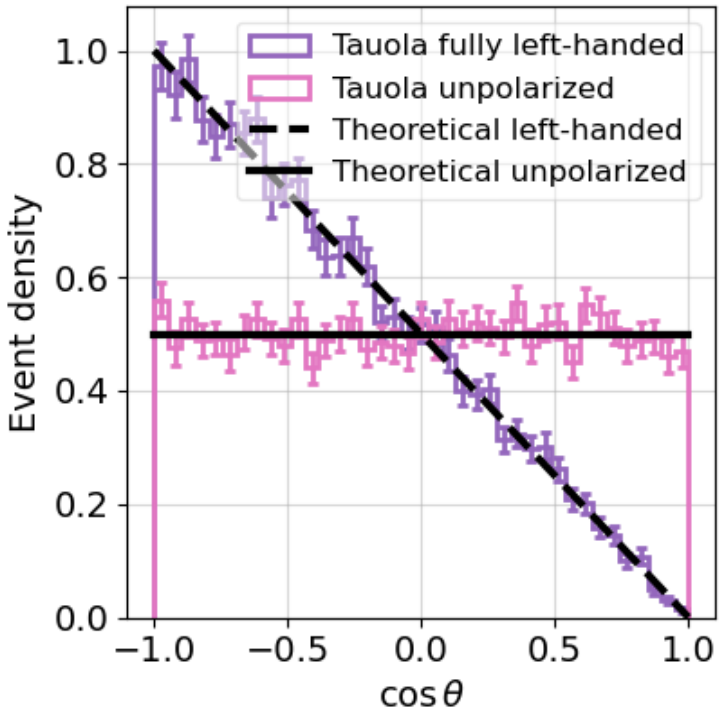

Figure 4.1: The π^- angle in the tau rest frame relative to the tau momentum direction. Note that since the tau does not have any momentum in the rest frame by definition, the angle is defined relative to the $+z$ direction. The colored distributions show the fully polarized left-handed ($P_L = -1$) and the unpolarized ($P_L = 0$) distributions given by simulated decays with TAUOLA, while the black lines show the theoretically predicted distributions. The polarized and unpolarized histograms contain 11165 and 11171 TAUOLA events respectively.

We now investigate the angular and energy distributions for the leptonic decay modes $\tau^- \to \mu^- \overline{\nu}_\mu \nu_\tau$ and $\tau^- \to e \overline{\nu}_e \nu_\tau$, in the tau rest frame. Since there are three decay products, the energy of the lepton is not deterministic, contrary to the two-body pion decay. We instead have a 2D distribution of the lepton energy and angle relative to the tau. The distribution is proportional to

$$\frac{\mathrm{d}\Gamma}{\mathrm{d}E\ \mathrm{d}\cos\theta}\left(\tau^- \to \ell^- \bar{\nu}_\ell \nu_\tau\right) \propto pE\left[3E_{\max} - 2E - \frac{m_\ell^2}{E} + P\cos\theta\frac{p}{E}\left(E_{\max} - 2E + \frac{m_\ell^2}{m_\tau}\right)\right], \tag{4.2}$$

where $l \in \{e, \mu\}$, p, E are the lepton momentum and energy respectively, $E_{max} = (m_\tau^2 - m_l^2)/(2m_l)$ is the maximum energy that the lepton can have in the tau rest frame [11]. The TAUOLA output distributions and the theoretical 2D distributions for the $\tau^- \to \mu^- \overline{\nu}_\mu \nu_\tau$ are shown in Figure 4.2. Both the fully polarized ($P_L = -1$) and unpolarized cases ($P_L = 0$) are included. Once again, we see good agreement between theory and the TAUOLA output.

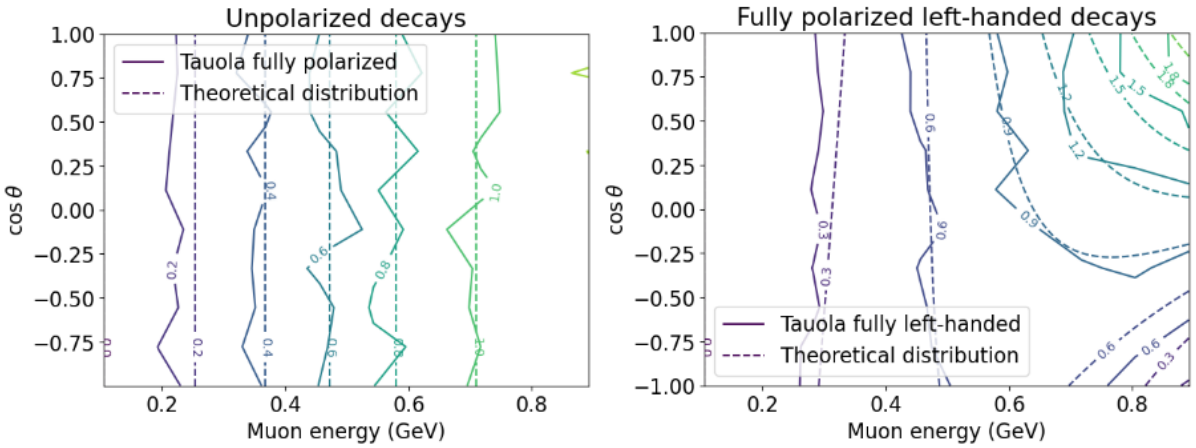

Figure 4.2: The muon energy and angle in the tau rest frame relative to the tau momentum direction, for the unpolarized ($P_L = 0$, left) and fully polarized ($P_L = -1$, right) cases. The full lines show contours for the TAUOLA distribution, while the dashed lines show the theoretical distribution. The histograms have been normalized such that the integral is 1. For TAUOLA, The unpolarized and polarized histograms contain 119420 and 119707 simulated muon decays respectively.

Lastly, we investigate the visible energy fraction distribution in the high-energy tau case, in the lab frame. For this, we look at the $\tau^- \to \pi^0\pi^-\nu_\tau$ decay mode. In Ref. [11], the energy fraction distribution of the visible decay products are shown for this decay mode in the collinear limit, i.e. when $E_\tau \gg m_\tau$ and all decay products move roughly in the same direction as the tau in the lab frame. This distribution is compared to the output of TAUOLA when simulating tau decays with a kinetic energy of 1000 GeV $\gg m_\tau \approx 1.777$ GeV). The outputs are shown in Figure 4.3. Here, we also see a good agreement between the theory and the TAUOLA distributions, within statistical uncertainties.

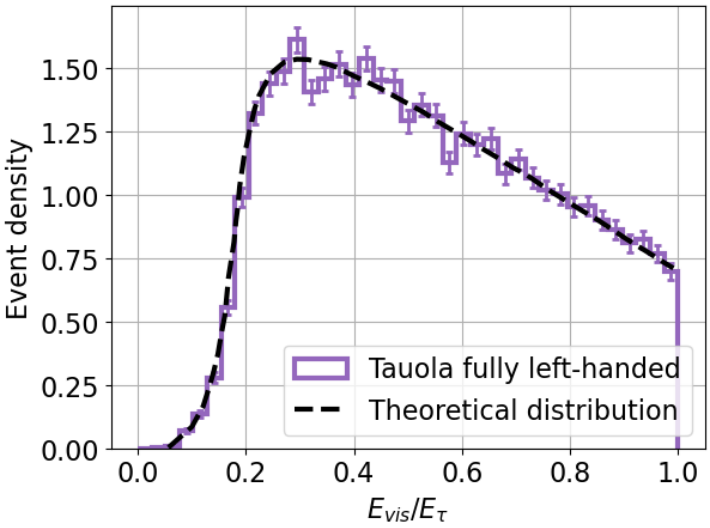

Figure 4.3: The hadronic energy fraction relative the the tau lepton for $\tau^- \to \pi^0\pi^-\nu_\tau$ decays. The distribution is shown in the lab frame for tau leptons with an energy of 1000 GeV. The stair-shaped distribution shows the fully polarized left-handed ($P_L = -1$) case given by TAUOLA simulations, while the dashed line shows the theoretically predicted distributions, extracted from Ref. [11].

In conclusion, these three comparisons show that the TAUOLA output agrees well with theory, both for distributions in the tau rest frame, the lab frame, for various decay modes, and for different polarization values. While not shown here, the same simulations have also been performed using PYTHIA8 and show good agreement. We therefore believe that the outputs of TAUOLA can be assumed to be correct.

4.2 Mono-energetic tau neutrinos with realistic polarization

We now show results for simulations with mono-energetic incoming tau neutrinos. Tau neutrino energies of 5, 10, 20, 50, and 100 GeV are simulated. In Figure 4.4, the energy distributions of the tau leptons are shown for the various incoming neutrino energies. One can see that as the energy increases, the number of DIS events increase, which also have the widest spread in the energy distribution of the tau energies. Contrary to this, the RES and QEL events result in a much more narrow energy distribution, closer to the incoming neutrino energy.

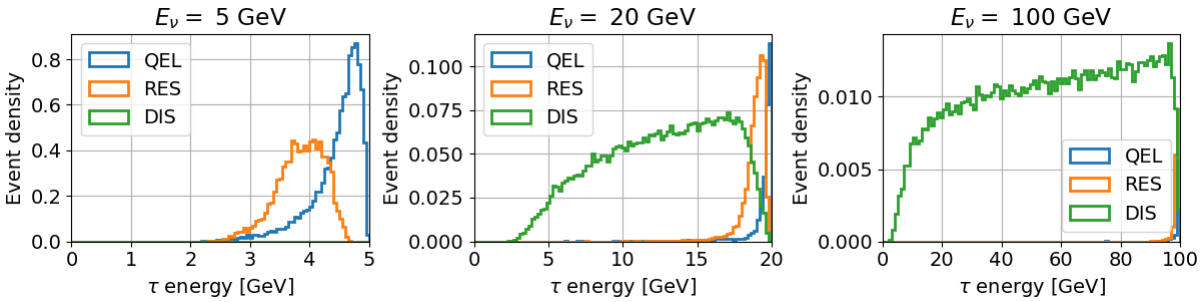

Figure 4.4: The energy distributions of the tau leptons produced by the tau neutrinos with different energies. The distributions are shown separately for QEL, RES and DIS events. Note that the histograms are normalized such that the sum of the integrals of the histograms add up to one.

4.2.1 Tau polarization validation

In this section, the results for calculating the tau polarization for tau neutrino-nucleus interactions with mono-energetic neutrinos are shown.

For validating that the calculation and implementation of the tau polarization are correct, Figure 6 in Ref. [12] was recreated, which is shown in Figure 4.5. For completeness, the original figure from Ref. [12] is also included in this thesis, as Figure 2.7. Comparing these two figures show that the polarization values from the implementation used in this study is generally in good agreement with what is seen in Ref. [12]. There are however some differences. Firstly, the polarization in Figure 4.5 does not follow a continuous line as a function of the tau energy, which it in theory should do, according to Figure 2.7. This is due to the random nucleon motion, which is not accounted for in Figure 2.7. Secondly, the RES scattering in particular has a large variance in the polarization, even with events that have the same tau energy. This is likely due to the fact that the RES polarization model used here accounts for different types of resonances, while the RES polarization model in Ref. [12] always assumes that the interaction produces the lightest resonance. Since a slightly different model is used for the RES polarization calculations, we also do not expect the polarization to perfectly match between Figure 2.7 and Figure 4.5. Additionally, we do not expect the DIS polarization to perfectly match between Figure 2.7 and Figure 4.5 either, as the PDFs and corrections used in Ref. [12] were not specified, and might therefore not be the Bodek-Yang corrected GRV98LO PDF set.

For QEL, the same formula for the tau polarization as the one used in Refs. [12] and [13] were used. Except for the variance caused by nucleon motion, we therefore expect the polarization to be identical, which we almost see. There are however a few events which have tau energies that are much lower than what is expected from QEL scattering. The origin of these events is unknown, but could be events generated by GENIE where the Björken x is not exactly 1, or due to a large nucleon momentum. The number of these types of QEL events is however a small fraction of the total QEL events, and an even smaller fraction of the total number of events simulated. We therefore expect their contributions and potential errors (if there is any) to be negligible. Furthermore, the apparent issue with these events come from the GENIE output of the tau energy, not

the tau polarization formula implemented in this thesis.

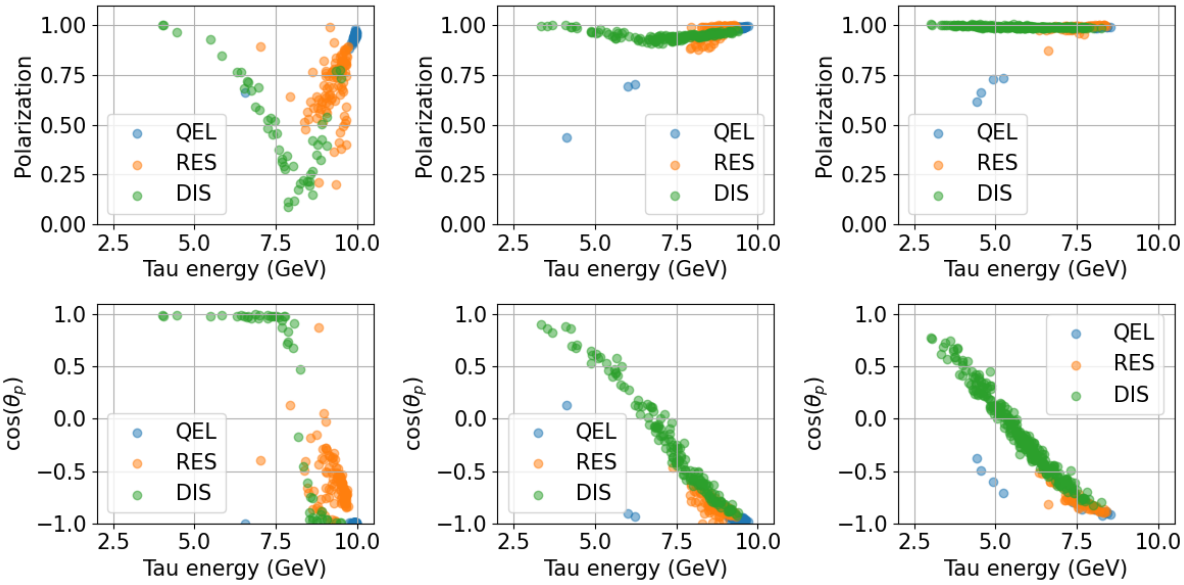

Figure 4.5: A recreation of Figure 6 in Ref. [12]. The top row shows the polarization magnitude of the tau lepton, while the bottom row shows the $\cos\theta_P$ of the polarization vector, i.e., how large the longitudinal component of the polarization is relative to the whole polarization vector. The left-most column shows interactions where the tau lepton outgoing angle relative to the incoming neutrino is 0°, the center column shows 5°, and the right column shows 10°. Different colored dots show events of different interaction types, as indicated by the legend in each figure. All events are simulated with an incoming neutrino energy of 10 GeV.

In Figure 4.6, the magnitude of the polarization vector and the angle between the polarization vector and the momentum vector is shown for all simulated mono-energetic tau leptons. We see that for all energy levels, most events are strongly polarized, with a polarization magnitude close to 1 and a $\cos\theta_P$ close to -1. However, at low E_ν, the $\cos\theta_P$ variance is non-negligible, especially for DIS and RES events. At $E_\nu = 5$ GeV, we even see that the majority of the RES events are right-handed rather than left-handed.

As the ν_τ energy increases, the polarization magnitude quickly approaches 1. For $\cos\theta_P$, the convergence towards -1 is slower, especially for DIS events. Another notable feature is that the RES polarization distributions are roughly in-between the QEL and DIS distributions. Since the different interaction types are different physical processes, there is no physical explanation for this, but a similar trend has been seen in earlier studies [12].

A few RES and DIS events were found to have a magnitude greater than 1. This is likely due to numerical errors rather than something physical. Furthermore, since it is such a small fraction ($\approx 1\%$) of events and the polarization magnitude is so close to 1 for these events, the error caused by the polarization mismodeling of these events is negligible. To make these polarization vectors physical, the vector is normalized to have a magnitude of 1 before being passed to TAUOLA.

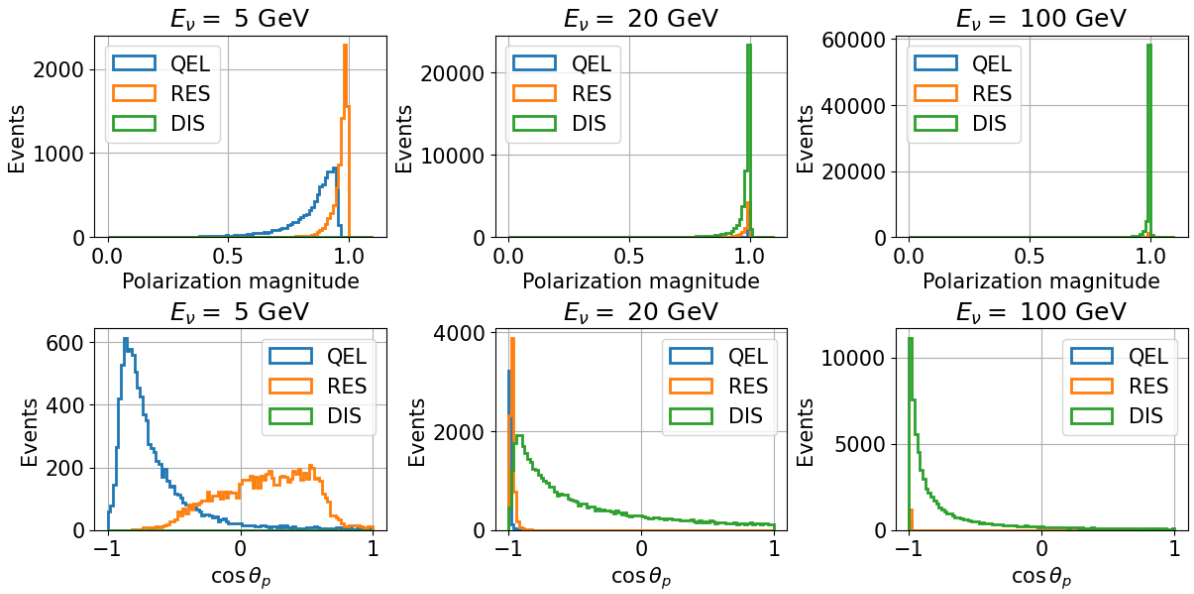

Figure 4.6: The distribution of the polarization magnitude (top row) and $\cos\theta_P$ (bottom row) for neutrino-nucleus interactions, with mono-energetic tau neutrinos. Each column shows a different incoming neutrino energy, with the lowest (5 GeV) to the left and highest (100 GeV) to the right. Different colors show different interaction types.

We now run tau decay simulations using TAUOLA for the realistic polarization that was calculated. This is then compared to the Geant4 outputs from the IceCube DeepCore tau decay simulations. For conciseness, only the neutrino energies of 5, 20, and 100 GeV will be shown. In reality however, simulations of all the energies listed earlier have been performed and analyzed.

4.2.2 Muon decay mode

First, the $\tau^- \to \mu^- \overline{\nu}_\mu \nu_\tau$ decay mode is investigated. This decay mode is of particular interest, as most track-like events in IceCube originate from the muon decay channel, whereas all other decay modes typically are identified as cascade-like events. Note however that this is not a perfect separation, as other decay modes are sometimes classified as track-like and vice versa, due to detector effects, low-energy muons that are not perfectly measured, and other imperfections in the track identification of IceCube.

The angular distributions of the muon relative to the mother tau lepton in the rest frame of the tau lepton is shown in Figure 4.7. This is a 1D projection on the y-axis of the 2D histogram in Figure 4.2.

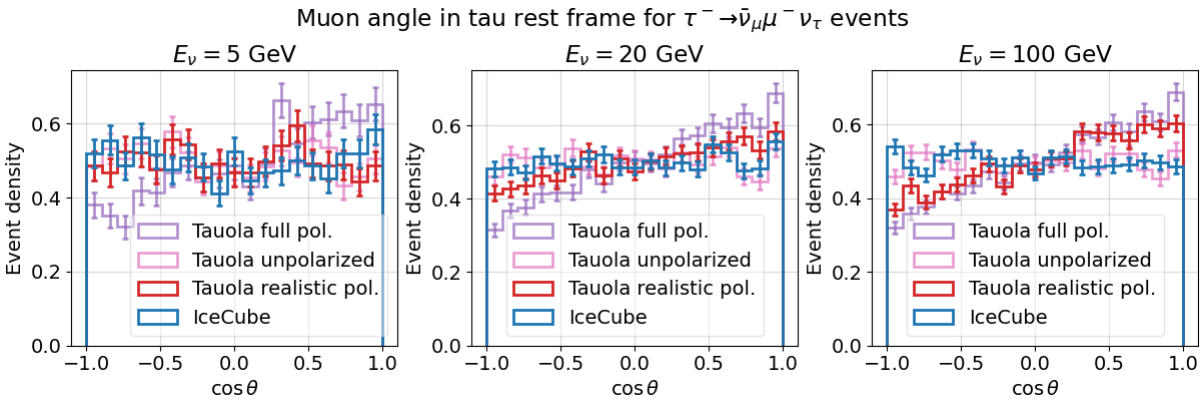

Figure 4.7: The $\cos\theta$ of the muon in the tau rest frame for $\tau^- \to \mu^- \overline{\nu}_\mu \nu_\tau$. Here, θ is the angle between the tau momentum and the muon momentum in the tau rest frame. Each subplot shows the distribution for different incoming neutrino energies, from 5 GeV (left) to 100 GeV (right). The different histograms in each subplot correspond to different tau decay simulations, with blue being the IceCube DeepCore simulations (based on Geant4), pink being the unpolarized tau decays using TAUOLA, purple being the fully polarized tau decays using TAUOLA ($P_L = -1$), and red being tau decays where the polarization is calculated analytically for each collision. The red distribution is the one that we expect to be the most correct.

When comparing the different distributions that have the same neutrino energy (e.g. the 100 GeV subplot), we see that the polarization has an effect on the angular distribution of the muon, which is precisely what we expect. For unpolarized decays (pink), the angular distribution is uniform, while for polarized decays (purple), muons tend to move in the same direction as the tau lepton. This is what we expect from the theory, since when the two neutrinos $\overline{\nu}_\mu, \nu_\tau$ move in the same direction, their spins will cancel out. This leads to the muon having to move in the same direction as the tau lepton for the total spin to be conserved. This is also what we observed in Figure 4.2.

Secondly, we also observe that the IceCube simulations are unpolarized, since the angular distribution agrees best with the TAUOLA unpolarized distribution. This is confirmed by the Geant4 documentation that states that polarization is not taken into account in tau decays [46]. When observing the TAUOLA simulations with a realistic polarization, we see that the distribution is consistently in between the TAUOLA unpolarized and TAUOLA fully polarized distributions. This is a good indication that the polarization is correctly accounted for in the TAUOLA simulations.

When comparing the different neutrino energies with each other, we see that all distributions except the one with the realistic polarization (red) do not change for different neutrino energies. This is expected, since the distributions shown are in the tau rest frame, and should therefore not be affected be the lab frame energy. The realistic polarization distribution does however change, since the calculated tau polarization depends on the incoming neutrino energy. We also observe that the realistic polarization distribution approaches the fully polarized distribution at higher neutrino energies, which is in agreement with our results in Figure 4.6. Note that the larger error bars at lower energies is due to the fact that there are fewer CC events out of the total simulated 100 000 events

(see Table 3.1).

One thing to note in Figure 4.7 is that the realistic polarization for events with $E_\nu = 5$ GeV is closer to the unpolarized distribution than the polarized one. This can be explained by viewing Figure 4.6, where we see that while QEL events generally are left-handed, the RES events are slightly right-handed at low neutrino energies. The combination of these two distributions likely result in a distribution similar to the unpolarized one.

We now show the energy distribution of the muon in the tau rest frame, which can be found in Figure 4.8. This is a projection of Figure 4.2 on the x-axis. Here, we see that there is almost no difference between the different polarization scenarios. This makes sense, as the polarization mainly affects the angular distribution of the decay products, rather than the rest frame energy of the decay products.

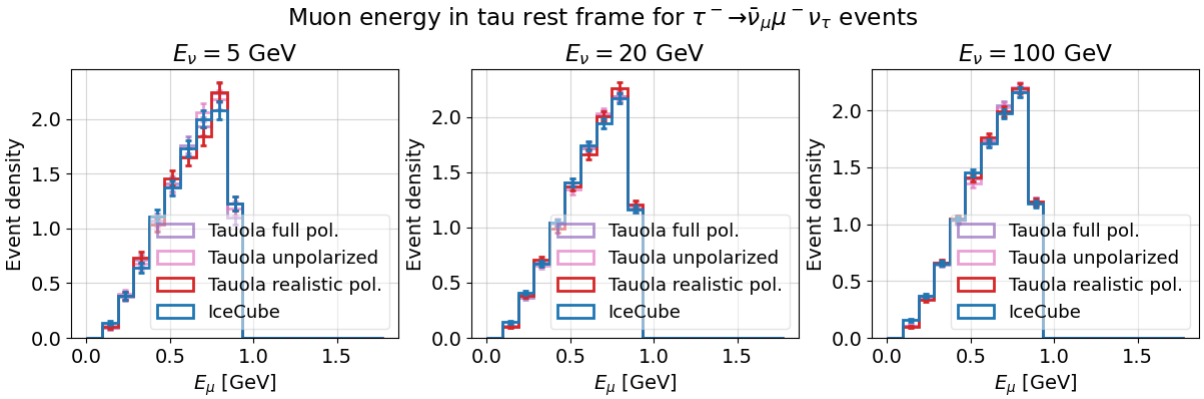

Figure 4.8: The energy that goes from the tau to the muon for $\tau^- \to \mu^- \overline{\nu}_\mu \nu_\tau$ in the tau rest frame. The figure format is the same as in Figure 4.7. Since this figure is in the rest frame, the maximum possible energy is $m_\tau \approx 1.777$ GeV.

When moving from the rest frame to the lab frame however, the different angles that the tau move in will affect the energy distribution. This is seen in Figure 4.9, where the energy fraction distribution of the muon relative to its mother tau lepton is shown. Here, a shift between polarized and unpolarized decays in the energy distribution can be seen for all neutrino energies, where the polarized tau decays result in a slightly more energetic muon. This is because the boost from the rest frame to the lab frame affects decay products moving at different angles relative to the tau in different ways. For polarized events, the muon generally moves in the same direction as the tau, which means that it gains more energy after the boost. For unpolarized tau decays, the muons are instead uniformly distributed relative to the tau momentum direction. The momentum of the muons moving in the opposite direction of the tau in the rest frame will instead counteract the boost. This causes the discrepancy in distribution between the polarized and unpolarized decays.

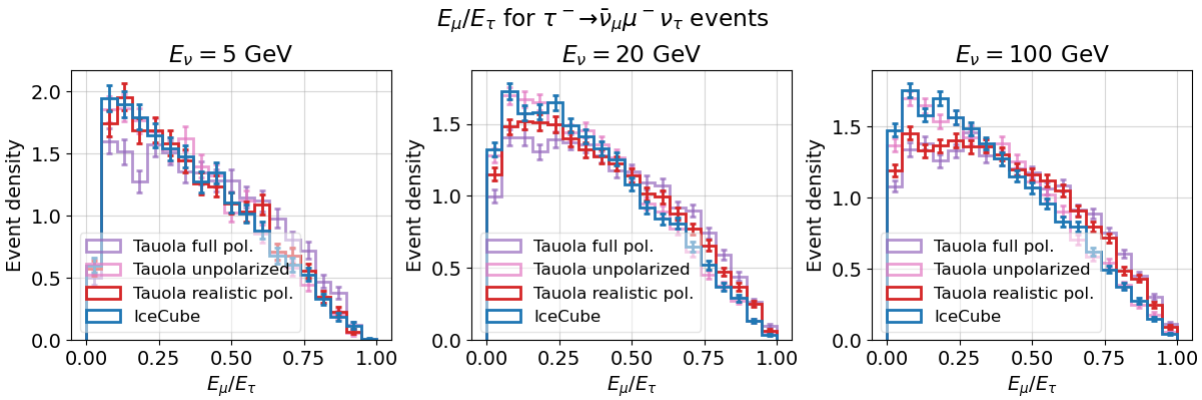

Figure 4.9: The fraction of energy that goes from the tau to the muon for $\tau^- \to \mu^- \overline{\nu}_\mu \nu_\tau$ decays. The figure format is the same as in Figure 4.11.

In Figure 4.10, the energy (note, not energy fraction) of the outgoing muon is shown. We see the same trend here as in Figure 4.9, where the polarized decays have a higher muon energy than the unpolarized decays. However, the deviation between the unpolarized and polarized decays is smaller. This can be explained by the fact that the outgoing tau leptons are not mono-energetic, but instead have varying energies ranging from the tau neutrino energy to almost no momentum, as seen in Figure 4.4. This results in a smearing of the distribution of the energy fraction, when converting to the absolute energy, which is what we see. This smearing has a greater effect at higher neutrino energies, since more taus are produced via DIS, which has a larger variance in the outgoing tau energy, as seen in Figure 4.4. This results in a smaller discrepancy between polarized and unpolarized decays at higher energies.

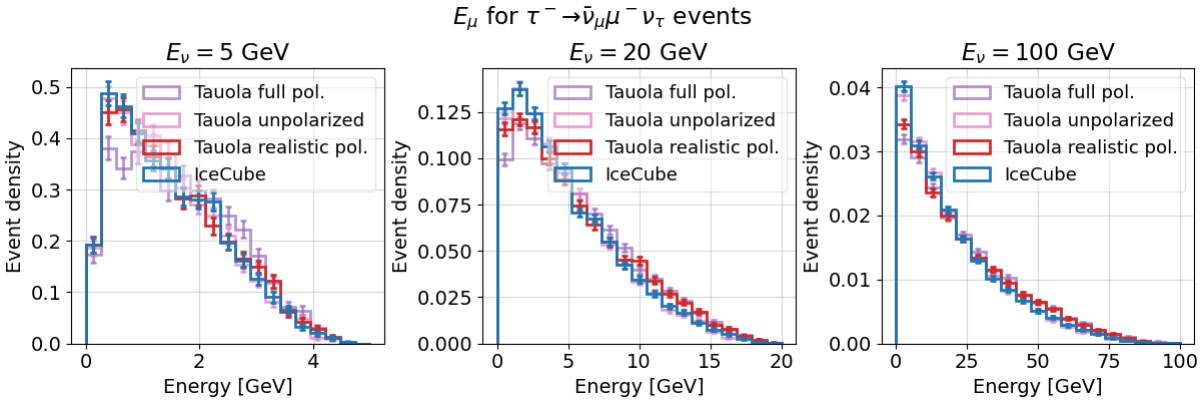

Figure 4.10: The absolute energy that the muon has in $\tau^- \to \mu^- \overline{\nu}_\mu \nu_\tau$ decays. Except for the x-axis, the figure format is the same as in Figure 4.9.

Lastly, we investigate the muon angle relative to the incoming neutrino in the lab frame, which is shown in Figure 4.11. We see a general trend where the muon is closer to the neutrino direction the more polarized the tau lepton is. This is explained by the fact that fully polarized tau neutrinos tend to move in the same direction as the tau lepton, which in turn is roughly moving in the same direction as the tau neutrino.

However, at higher energies, all particles are boosted in the neutrino direction to such a degree that the discrepancy between the different polarization values become negligible. Similar trends were also seen for all other decay modes. Consequently, this discrepancy is assumed to be negligible for the purposes of this study and the angular distributions in the lab frame will not be shown for other decay modes.

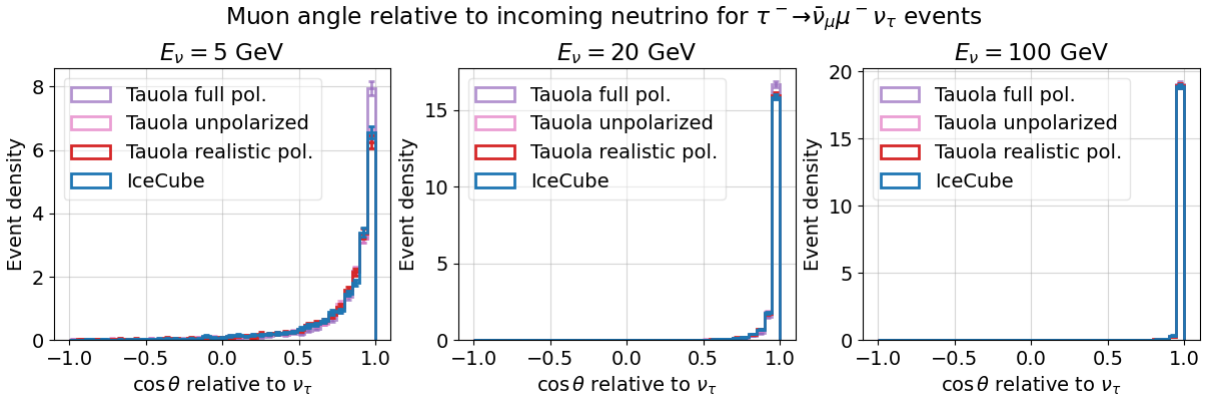

Figure 4.11: The distribution of the angle between the incoming tau neutrino and the outgoing muon that forms from $\tau^- \to \mu^- \overline{\nu}_\mu \nu_\tau$ decays. The figure format is the same as in Figure 4.9.

4.2.3 Single pion decay mode

We now investigate the $\tau^- \to \pi^- \nu_\tau$ decay mode. Since the pion is spin 0 and the neutrino is always left-handed, the neutrino will typically move in the same direction as the polarization of the tau lepton, in order to conserve the spin. This means that for fully left-handed tau decays, the neutrino typically moves in the same direction as the tau momentum direction, which due to conservation of four-momentum means that the pion moves anti-parallel to the tau lepton, in the tau rest frame. When boosting to the lab frame, this means that the π^- typically has less than half of the tau energy. For unpolarized decays however, the pion is emitted in any direction without considering the tau momentum, and therefore its energy fraction distribution is uniform. This is what is seen in Figure 4.12, where there is a large pion energy fraction distribution discrepancy between the fully polarized and unpolarized decays.

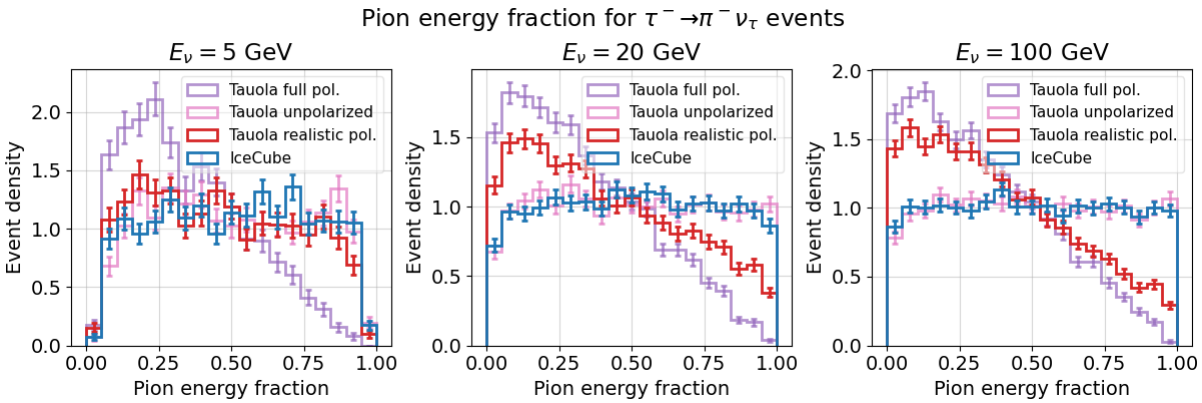

Figure 4.12: The fraction of energy that goes from the tau to the π^- in $\tau^- \to \pi^- \nu_\tau$ decays. The figure format is the same as in Figure 4.9.

When converting from the energy fraction (Figure 4.12) to the absolute visible energy (Figure 4.13), we see the same pattern but less pronounced. This is again due to the smearing, caused by the variety of tau energies that come out from the neutrino-nucleus interactions, even when the incoming neutrino is mono-energetic. However, contrary to the muon decay mode, the energy discrepancy is not negligible. Even for higher incoming neutrino energies than what is shown in Figure 4.13, the discrepancy remains roughly the same.

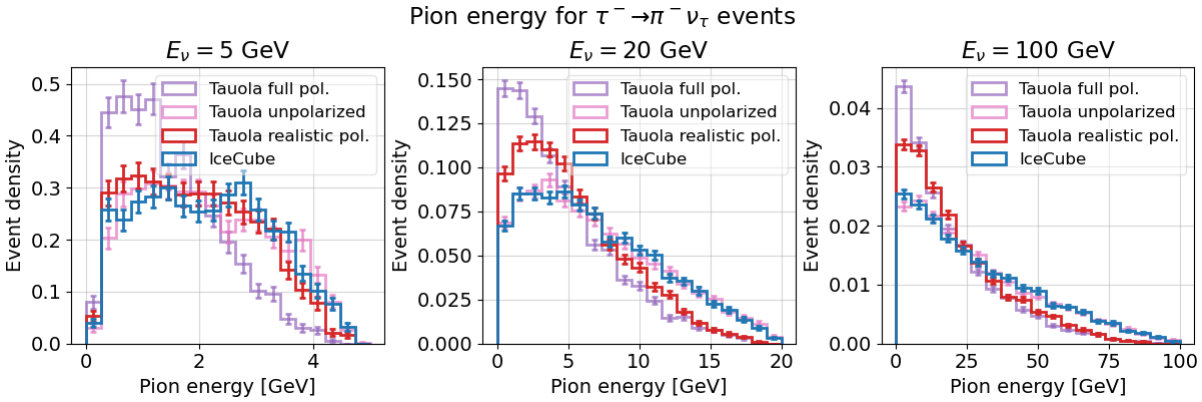

Figure 4.13: The absolute energy that the π^- has in $\tau^- \to \pi^- \nu_\tau$ decays. The figure format is the same as in Figure 4.10.

4.2.4 Decay modes with multiple hadrons

We now investigate the visible energy fraction for tau decay modes with multiple pions, more specifically $\tau^- \to \pi^- \pi^0 \nu_\tau$, $\tau^- \to \pi^- \pi^0 \pi^0 \nu_\tau$, and $\tau^- \to \pi^- \pi^- \pi^+ \nu_\tau$. Together, these decay modes constitute roughly 44% of all decays of the tau lepton. Note that the visible energy is now defined as the sum of the energies of all hadronic decay products.

In Figure 4.14, the visible energy fraction is shown for the $\tau^- \to \pi^- \pi^0 \nu_\tau$ decay mode. We see a larger discrepancy between the polarized and unpolarized TAUOLA decays for lower energy neutrinos, which is expected. However, strangely, the distribution from

the DeepCore simulations does not match any of the TAUOLA simulations, but instead grossly overestimates the visible energy fraction. A similar pattern is seen for the other hadronic n-body decay modes, as shown in Figure 4.15 and Figure 4.16. Based on the fact that it significantly deviates from the unpolarized TAUOLA output, this does not seem to be a polarization issue but rather something else.

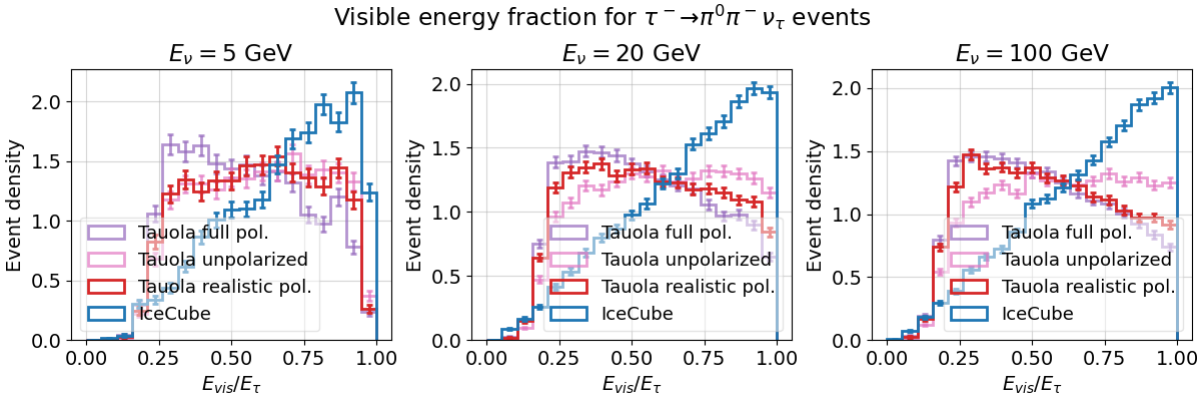

Figure 4.14: The fraction of energy that goes from the tau to the pions in $\tau^- \to \pi^-\pi^0\nu_\tau$ decays. The figure format is the same as in Figure 4.9.

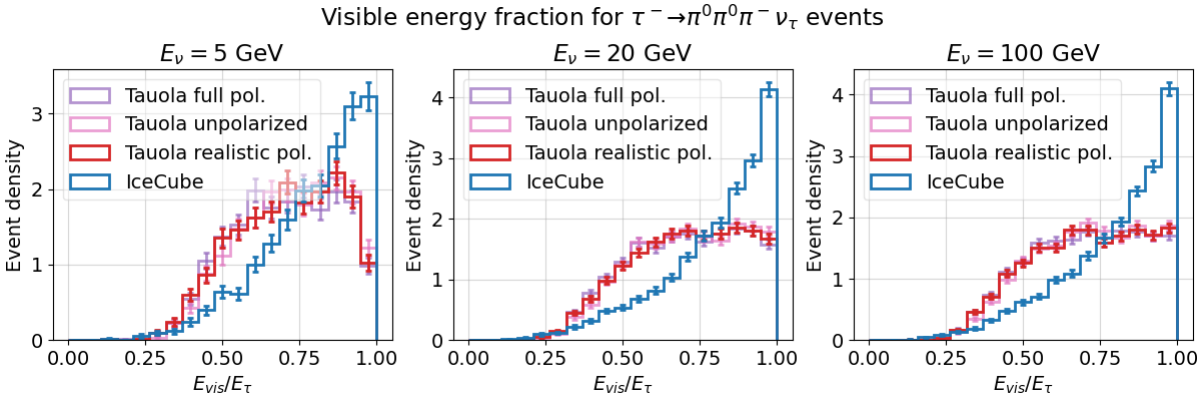

Figure 4.15: The fraction of energy that goes from the tau to the pions in $\tau^- \to \pi^-\pi^0\pi^0\nu_\tau$ decays. The figure format is the same as in Figure 4.9.

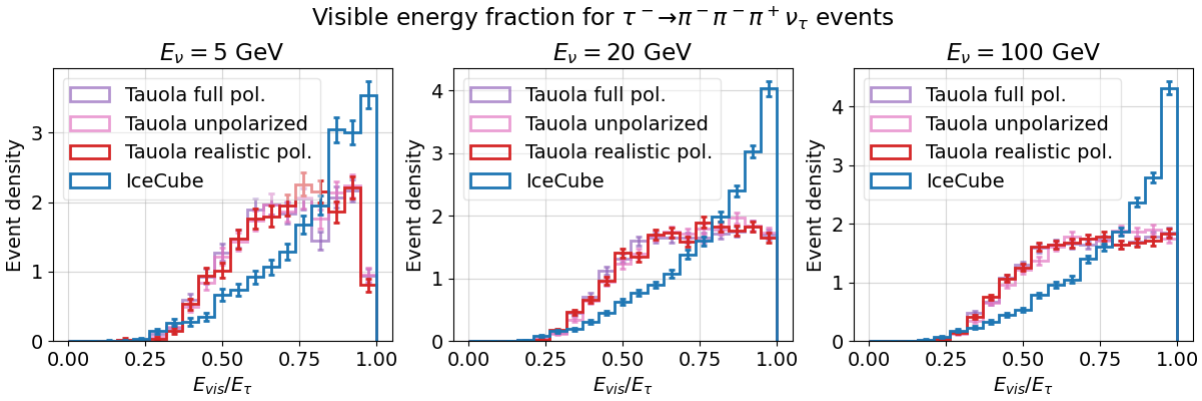

Figure 4.16: The fraction of energy that goes from the tau to the pions for $\tau^- \to \pi^-\pi^-\pi^+\nu_\tau$ decays. The figure format is the same as in Figure 4.9.

The cause for this was discovered to be that the Geant4 decay simulations do not take hadronic resonances into account. The effect of this intermediate resonance step, which is correctly simulated in TAUOLA, is that the momentum is divided equally between the resonance meson and the outgoing tau neutrino. In contrast, in Geant4, a n-body decay is simulated, where the four-momentum is divided among the tau neutrino and all the final state mesons. This naturally leads to a larger fraction of the energy being passed to the mesons, which results in the distribution discrepancy seen in the figures above, where the DeepCore (Geant4) simulations overestimate the visible energy fraction.

Clear evidence for the resonance in the TAUOLA simulations, and lack thereof in the IceCube DeepCore simulations can be shown by plotting the invariant mass distribution of the hadronic decay products. This is shown in Figure 4.17, where clear resonance peaks are visible for the TAUOLA decays, while there is no such peak for the Geant4 decays. Note also that the polarization does not affect the invariant mass distribution for the TAUOLA decays, since they are unrelated phenomena.

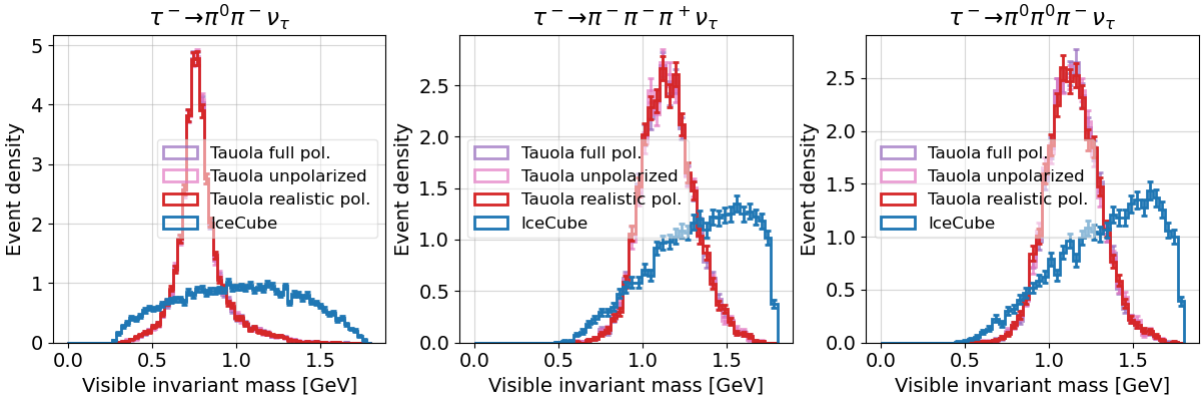

Figure 4.17: The invariant mass of the pions for $\tau^- \to \pi^-\pi^0\nu_\tau$ (left), $\tau^- \to \pi^-\pi^-\pi^+\nu_\tau$ (center) and $\tau^- \to \pi^-\pi^0\pi^0\nu_\tau$ (right). The simulated tau neutrinos have an energy of 100 GeV, though the distribution is identical for all other neutrino energies, since the mass is Lorenz invariant.

We now investigate how this affects the visible energy distribution, which is shown in Figures 4.18, 4.19 and 4.20. Like with the polarization effect for pions and muons, the discrepancy is greater in the energy fraction compared to the absolute energy distributions. However, the discrepancy caused by lack of resonances still has a non-negligible effect on the distributions.

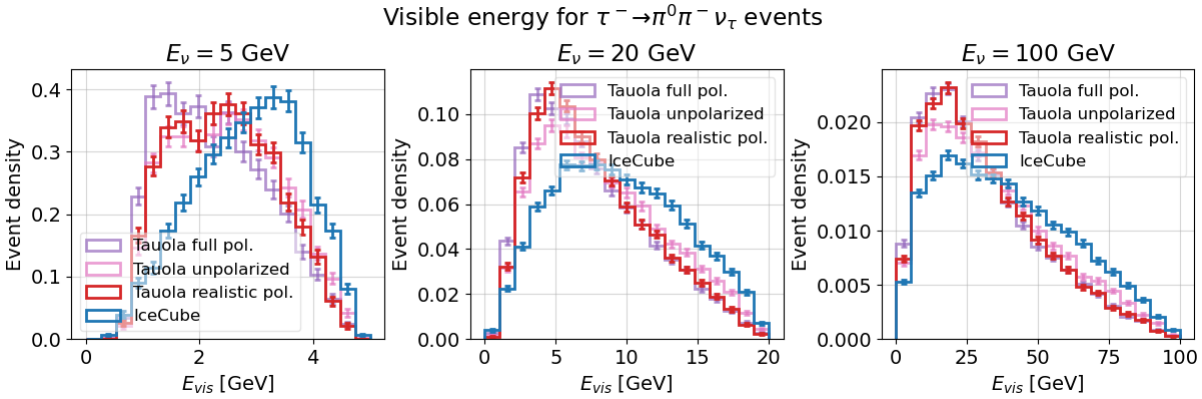

Figure 4.18: The visible energy for $\tau^- \to \pi^-\pi^0\nu_\tau$ decays. The figure format is the same as in Figure 4.10.

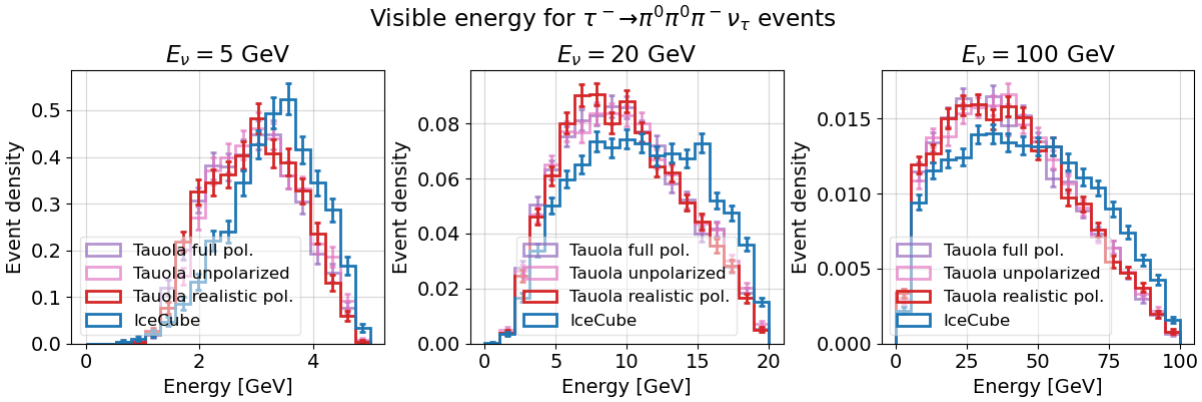

Figure 4.19: The visible energy for $\tau^- \to \pi^-\pi^0\pi^0\nu_\tau$ decays. The figure format is the same as in Figure 4.10.

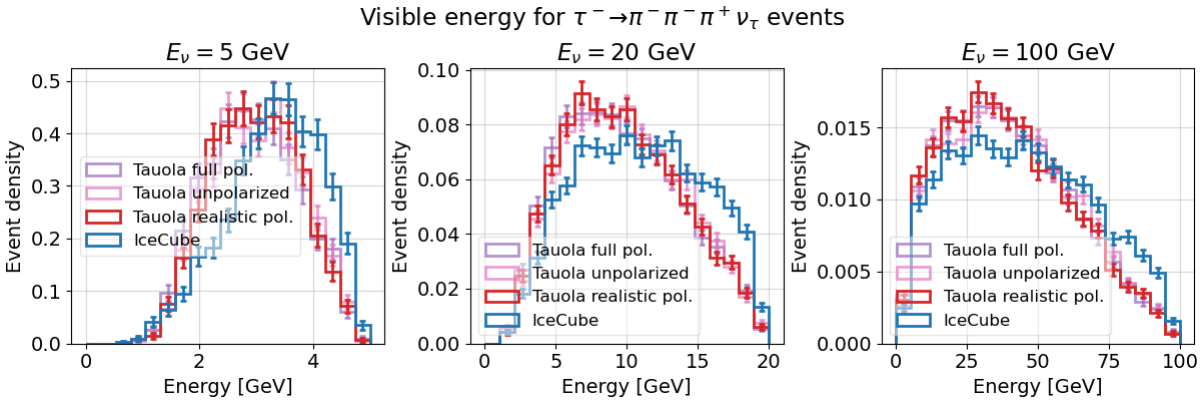

Figure 4.20: The visible energy for $\tau^- \to \pi^-\pi^-\pi^+\nu_\tau$ decays. The figure format is the same as in Figure 4.10.

4.2.5 Missing decay modes

During this study, it was discovered that roughly 13% of the tau decay modes are not implemented in Geant4. The energy distributions for these are shown in Figure 4.21. We clearly see that the visible energy fraction for the missing decay modes is shifted towards 1, and generally higher than all the previously investigated decay modes. This is because a majority (approximately 74%) of the missing decay modes are hadronic, with the rest being $\tau^- \to e^-\nu_\tau\overline{\nu}_e\gamma$ (22%) and $\tau^- \to \mu^-\nu_\tau\overline{\nu}_\mu\gamma$ (4%). Note that the percentages written here are relative to the missing decay modes, not relative to the total branching ratio. Since hadronic decay modes tend to have a large visible energy fraction (as seen in Figures 4.14–4.16), while leptonic decays have a small visible energy fraction (as seen in Figure 4.9), the dominance of the hadronic decay modes explain the shift towards higher visible energy fractions Figure 4.21.

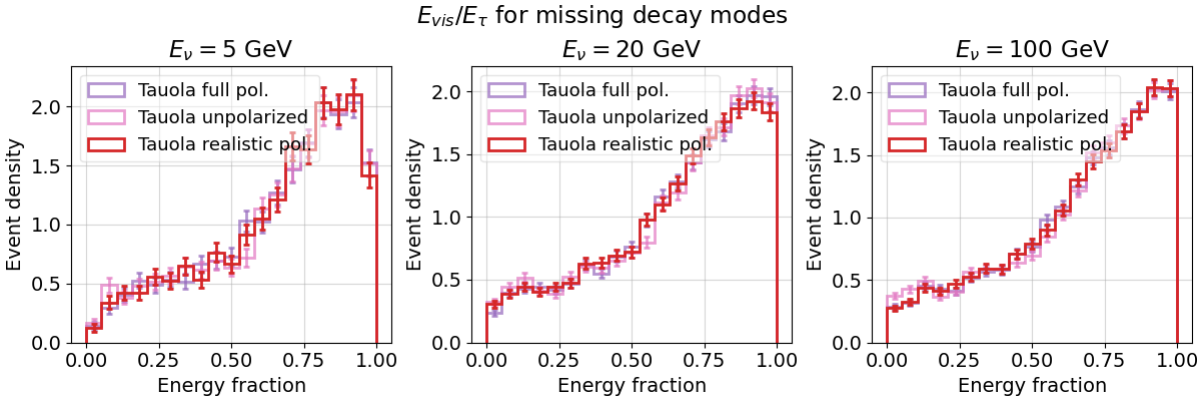

Figure 4.21: The visible energy fraction distribution for the decay modes that are not implemented in Geant4. The figure format is the same as in Figure 4.9, but no IceCube distribution is shown.

4.2.6 Cascade-like events

We now combine all decay modes that are cascade-like, i.e. all decay modes that do not contain muons. As noted earlier, this is not a perfect classification, as events can be misclassified during reconstruction. However, it serves as a rough approximation of what the expected discrepancy between the correct tau decay simulations and the current Geant4-based decay simulations are like. Figure 4.22 shows the visible energy fraction, while Figure 4.23 shows the absolute visible energy for various incoming neutrino energies.

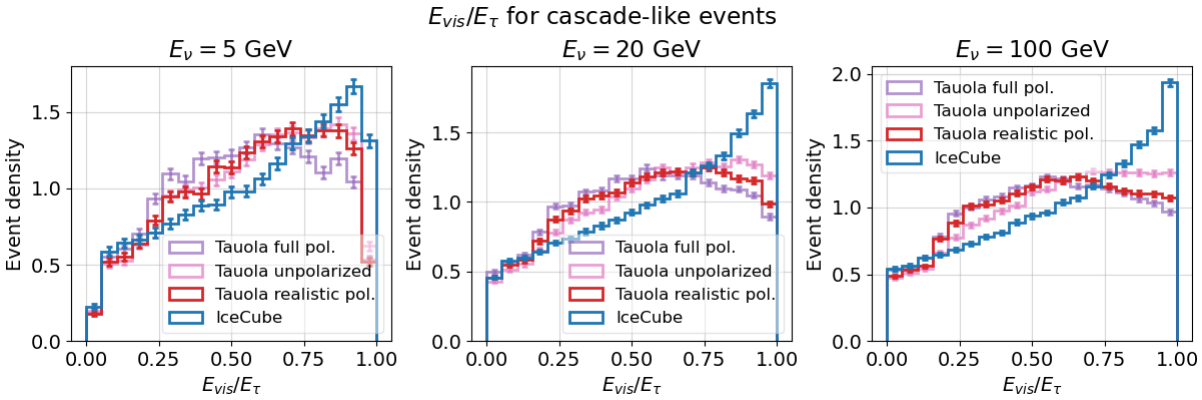

Figure 4.22: The visible energy fraction distribution for all cascade-like decay modes, i.e., all decay modes without muons. The figure format is the same as in Figure 4.9.

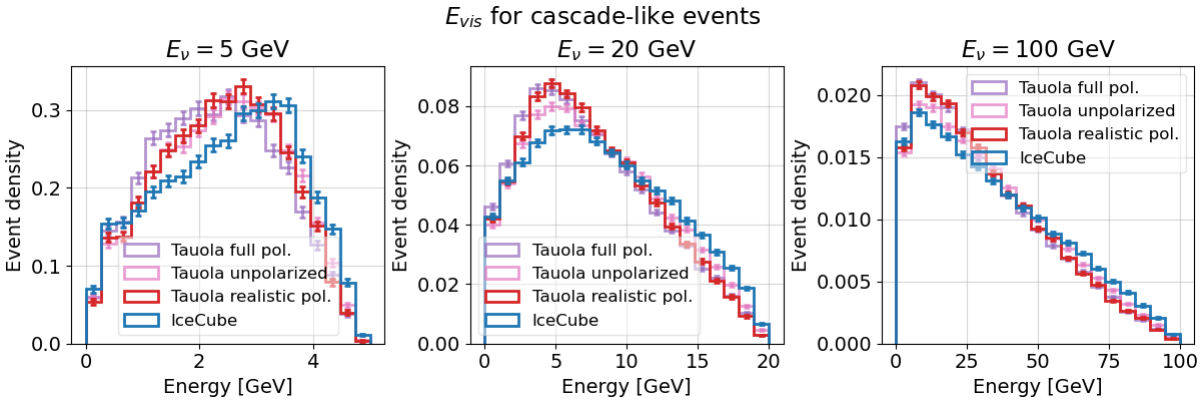

Figure 4.23: The visible energy distribution for all cascade-like decay modes, i.e., all decay modes without muons. The figure format is the same as in Figure 4.10.

We see that the discrepancy between the TAUOLA decays with realistic polarization and Geant4 decays is smaller than when comparing individual hadronic decay modes. This is mainly due to the electron decay modes being included, since the electron decay mode has a small discrepancy between the IceCube and TAUOLA. Still, a clear shift in the distributions can be seen.

4.2.7 PROPOSAL

While PROPOSAL has not been used to run simulations in this thesis, comparisons with available energy fraction distributions in Ref. [8] have been performed. In Figure 4.24, visible energy fraction distributions, both in the lab frame and in the rest frame, are shown for the hadronic decay modes.

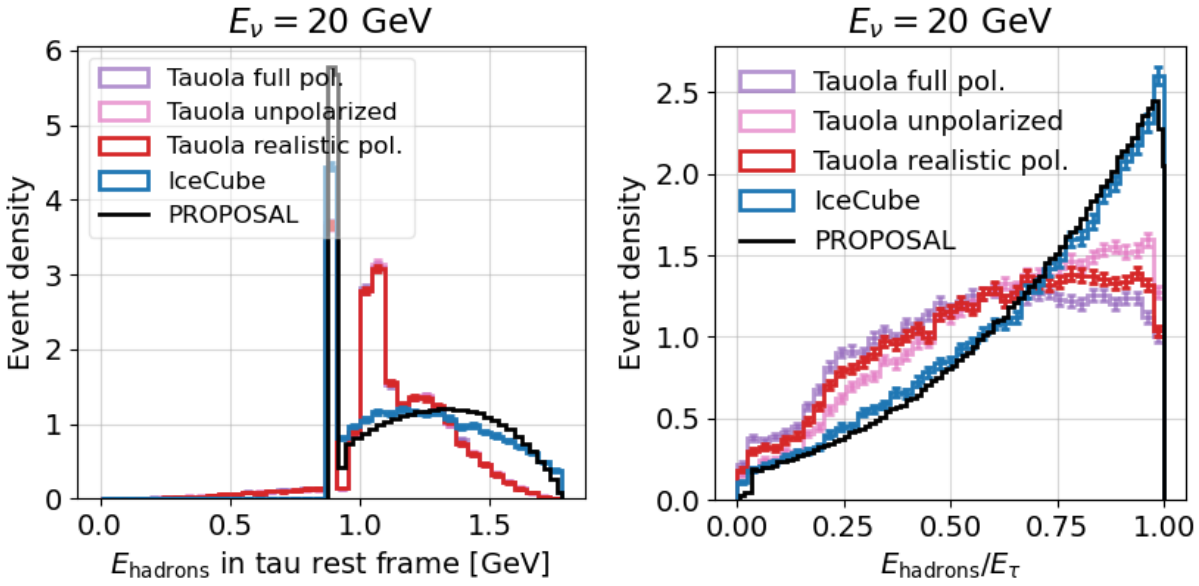

Figure 4.24: The energy fraction of the tau lepton that goes to hadrons for all hadronic decays. The left plot shows the tau rest frame, while the right plot shows the lab frame. The incoming neutrino energy shown is for 20 GeV. The PROPOSAL distributions are taken from Ref. [8] Figure 5. The figure format is the same as in Figure 4.9.

We see that the PROPOSAL distributions much better with the Geant4 distributions than the TAUOLA distributions. This clearly shows that n-body decays are used in PROPOSAL in a similar way as in Geant4. This also confirms what is stated in Ref. [8]. The slight deviations between the PROPOSAL and Geant4 distributions can likely be attributed to two factors. First, the neutrino or tau energy used for the PROPOSAL simulations was not stated in Ref. [8], and the comparison between the PROPOSAL distributions and the other distributions in Figure 4.24 might therefore not be completely accurate. However, the energy fraction distributions are relatively similar for all incoming neutrino energies $\gtrsim 3$ GeV. As long as the tau energies are $\lesssim 3$ GeV for the PROPOSAL simulations, the distributions should be roughly comparable. Secondly, PROPOSAL has more decay modes implemented than Geant4 [8], most of which are hadronic, which also results in a slight difference between the distributions.

We also compare the hadronic energy distribution in the lab frame between TAUOLA and an older version of PROPOSAL, when hadronic resonances were implemented. This is shown in Figure 4.25. While there is a discrepancy between the old PROPOSAL distribution and the TAUOLA unpolarized distribution, they are relatively similar to each other when compared to the distribution from the current PROPOSAL version which

utilized n-body decays.

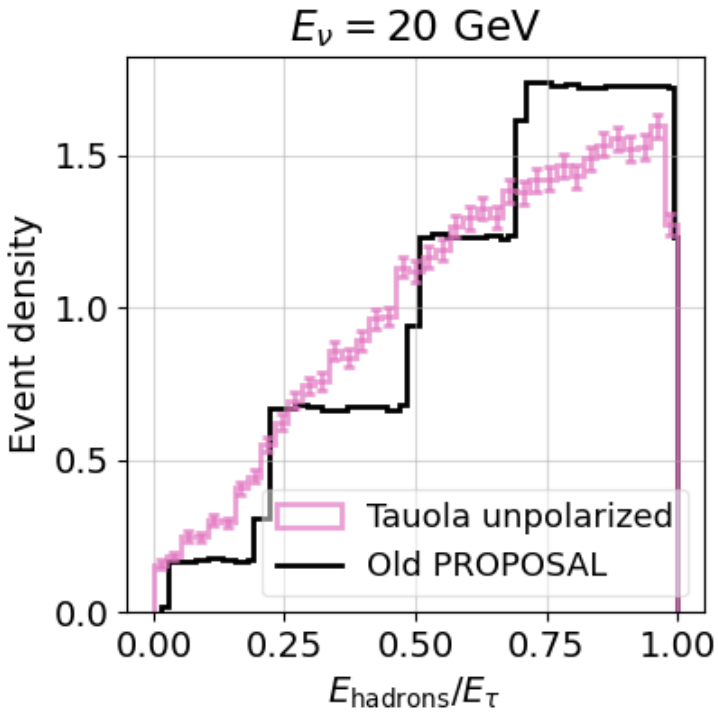

Figure 4.25: The energy fraction of the tau lepton that goes to hadrons for the hadronic decays in the lab frame. The figure format is the same as in Figure 4.24.

4.2.8 Erroneous decay modes

In this section, the discrepancies shown in the previous sections are summarized in a table. In Table 4.1, all the decay modes of the tau lepton and how much they differ between Geant4, PROPOSAL and the realistic TAUOLA polarization are listed. The main two causes for discrepancies is that neither hadronic resonances nor polarization are taken into account in the current decay simulations. Geant4 simulations are further affected by the fact that only six decay modes are implemented, and some decay modes are also missing from PROPSAL (though with a smaller effect).

Decay mode	$\mathcal{BR}$	Geant4 $\mathcal{BR}$	PROPOSAL $\mathcal{BR}$	Problem
$\pi^-\nu_\tau$	11.1	12.3	11.5	Major polarization issue
$\mu^-\overline{\nu}_\mu\nu_\tau$	17.1	18.9	17.4	Minor polarization issue
$e^-\overline{\nu}_e\nu_\tau$	15.2	19.8	17.8	Minor polarization issue
$\pi^-\pi^0\nu_\tau$	25.3	28.3	26.0	No resonance
$\pi^-\pi^0\pi^0\nu_\tau$	9.2	10.2	9.5	No resonance
$\pi^-\pi^-\pi^+\nu_\tau$	8.9	10.6	9.8	No resonance
$\pi^-\pi^-\pi^+\pi^0\nu_\tau$	4.6	0	4.6	Not implemented in G4
$e^-\overline{\nu}_e\gamma\nu_\tau$	2.9	0	0	Not implemented
Other	5.8	0	3.4	Not implemented in G4

Table 4.1: A summary of all decay modes and how the DeepCore decay simulations of each decay mode differ from TAUOLA decays with a realistic polarization. The first column shows the decay products for a specific decay mode, the second column shows the branching ratio of the decay mode (in %, calculated empirically using 68853 TAUOLA events), the third column shows the branching ratio that Geant4 gives (also calculated empirically, using the same number of events), the third column shows the branching ratio given by PROPOSAL (taken from the source code [47]), and the last column shows the greatest cause for a discrepancy between the energy distribution for TAUOLA decays with a realistic polarization, and the DeepCore decays. "Major polarization issue" means that there is a non-negligible discrepancy between polarized and unpolarized decays. "Minor polarization issue" means the same thing but that the discrepancy is relatively small. "No resonance" means that resonances are not simulated, "Not implemented" means that neither Geant4 nor PROPOSAL has the decay mode implemented, and "Not implemented in Geant4" means that it is implemented in PROPOSAL but not in Geant4.

Chapter 5

Discussion and conclusions

5.1 Discussion

From the results above, we can draw the conclusion that all decay modes are affected by mismodeling. The problems can be characterized into three categories: polarization, resonance decays, and missing decay modes. In this section, we discuss these three problems, their interplay and the implications.

5.1.1 Polarization effects

From Figure 4.6, we can see that the polarization typically has a greater variance for low-energy incoming tau neutrinos, with the polarization approaching fully left-handed polarization at higher energies. This agrees with theoretical expectations, where at energies $\gg m_\tau$, we expect the helicity to be the same as the chirality. Since the taus are only produced through weak interactions, the helicity should therefore approach a left-handed state. However, we also see that even for tau neutrinos with energies of 100 GeV, there is a relatively large variance of the polarization angle θ_P. This is likely explained by the fact that at these energies, DIS interactions dominate, which, as seen in Figure 4.4, has a large and almost uniform distribution of the produced tau lepton energy. Consequently, even for high-energy neutrinos, there are a non-negligible number of low-energy tau leptons produced, which then can have a polarization that is not fully left-handed.

We see in the energy distributions above that the polarization mainly affects decay modes with few particles, namely leptonic decays and the hadronic decay modes $\tau^- \to \pi^-\nu_\tau$ and $\tau^- \to \pi^0\pi^-\nu_\tau$. This is because the tau polarization affects the direction that the particles are allowed to move in, in order to conserve spin after the decay of the tau. For decays with more than three particles, i.e., most hadronic decay modes, there are many degrees of freedom, and the spin conservation therefore only has a small effect. This is clearly seen in e.g. Figure 4.15, where the discrepancy between the TAUOLA fully polarized and TAUOLA unpolarized decays are negligible. Furthermore, the decay mode affected the most by polarization is $\tau^- \to \pi^-\nu_\tau$, as can be seen in Figures 4.12.

Another interesting aspect with the polarization is that the energy distribution is shifted towards higher energies for leptonic decay modes (Figure 4.2) , while the opposite is seen for hadronic decays (Figure 4.12). This makes sense, since the tau polarization

is mostly left-handed, and to conserve the spin, the leptons are favored to move in the same direction as the tau lepton. On the other hand, for hadronic decay modes, pions have spin 0, and to conserve spin, the neutrinos should instead move in the direction of the tau lepton. When boosting the particles to the lab frame, the leptons are boosted in the same direction as they are already moving in, while the pions are boosted in the opposite direction. This then leads to the increased energy for leptons (as seen in e.g. Figure 4.9), and decreased energy for the hadronic decays (as seen in e.g. Figure 4.12).

We now compare the discrepancies for different incoming neutrino energies. Since the polarization gets more extreme and more left-handed at higher neutrino energies, this results in a greater discrepancy between the current IceCube DeepCore simulations and the realistic polarization decays, as seen mainly in Figures 4.12 and 4.9. However, DIS also dominates more at higher neutrino energies, which results in the tau energies being more spread out, and consequently the energy (not energy fraction) distribution discrepancies are more smeared out. These two effects are in tension, and as a consequence of this, it is difficult to say at which neutrino energies the energy discrepancy caused by polarization is the largest. By looking at Figure 4.13 however, it seems that generally the effect is greater for higher energies.

We can therefore conclude that the effects of the mismodeling of, or rather lack of consideration for polarization, is mixed. The effect that it has depends on both the incoming neutrino energy and the decay mode. Track-like events mostly consist of muons, and from this study we can conclude that the energy of the muons is slightly underestimated compared to the real energy that we expect, when taking polarization into account. This means that the light emitted from the muons is slightly brighter in reality than what the current IceCube DeepCore simulations predict. However, this effect is likely relatively small.

For cascade-like events, the situation is more complex. For the electron decay mode, the situation is the same as for the muons, i.e., the light emitted should be slightly brighter in reality than what current simulations predict. However, for the $\tau^- \to \pi^-\nu_\tau$ decay mode, the pion energy is typically overestimated by the current IceCube simulations. This means that the cascades in reality will on average be less bright than what we expect from the IceCube simulations. Consequently, the energy of reconstructed simulated events are currently being overestimated in IceCube.

For the energy scales of > 5 GeV that is of interest for IceCube, the angular distribution discrepancy caused by polarization for tau neutrinos seems to be negligible, as seen in Figure 4.11. This is due to the fact that the tau lepton momentum in the lab frame is much greater than the decay product momenta in the tau rest frame, and as such, after boosting to the lab frame, all decay products move roughly in the direction of the tau, regardless of their angle relative to the tau in the rest frame.

For even higher energy scales, far above atmospheric neutrinos used for oscillation studies and instead used to search for astrophysical neutrinos, the polarization still poses a problem. For these tau neutrinos, which have energies on the TeV scale, the produced tau is almost completely left-handed. However, PROPOSAL, which handles the decay of the tau lepton at high energies, currently does not take polarization into account. This means that the energy of the pion for $\tau^- \to \pi^-\nu_\tau$ decays would be overestimated. A fix for this has been proposed and implemented before [48], but is not included in the

main PROPOSAL software distribution. This fix always assumes the tau lepton to be fully left-handed, and does not support full polarization calculations. However, since the incoming neutrinos have such a high energy for the use cases of PROPOSAL, this approximation is reasonable.

5.1.2 Resonances

In Table 4.1, we can see that the largest discrepancy between TAUOLA and the current IceCube decay simulations is caused by the resonances not being taken into account in the Geant4 tau decay implementation. This affects all decay modes with two or more hadrons in the final state, which amounts to roughly 49% of the tau branching fraction. A resonance decay can in reality be seen as a two-body decay, where half of the momentum goes to the resonance particle and half of the momentum goes to the neutrino. The resonance particle will then decay to multiple pions (possibly going through another resonance, e.g. $a_1 \rightarrow \rho\pi$), where the resonance momentum is shared among these hadrons. When an n-body decay is simulated directly, the momentum and energy is instead directly divided among the n particles, resulting in a much larger fraction of the tau energy being transferred to the hadrons compared to a two-body resonance decay. This is why in Figures 4.14, 4.15, and 4.16, the tau energy fraction that goes to the hadrons is much greater for the IceCube DeepCore simulations than for the unpolarized TAUOLA decays (and for the TAUOLA decays with a realistic polarization, which for these decay modes is similar to the unpolarized case, as described in the previous section) which take resonances into account.

The resonance decay distribution discrepancy is, similar to the polarization discrepancy, slightly reduced in scale when viewing the absolute visible energy (Figures 4.18, 4.19, and 4.20) rather than the visible energy relative to the tau energy (Figures 4.14, 4.15, 4.16). This is once again caused by the smearing, due to the wide range of tau lepton energies, especially for high-energy neutrinos. The combination of these two effects means that the largest discrepancy caused by resonances is roughly around neutrino energies of 10 GeV.

What is common for all the resonance decay discrepancies is that the visible energy is overestimated with the current simulations, which means that the light emitted in IceCube DeepCore is dimmer than what the current IceCube simulations predict. Furthermore, all of these decay modes are connected to the cascade-like events, which means that cascade-like events are mismodeled the most, as seen when comparing e.g. Figure 4.9 and Figure 4.22.

The discrepancy described above is not only a problem for oscillation studies but also for astrophysical tau neutrino searches. This is because hadronic decays of tau leptons through resonance decays were replaced with n-body decays in 2018 [8]. The motivation for this was because the resonance decays resulted in step functions in the energy fraction, with each step corresponding to different resonances, as can be seen in Figure 4.25. These step functions were seen as unphysical and instead replaced with the n-body decays, which results in a continuous energy distribution [8]. As can be seen from the same Figure however, the step functions are not present in TAUOLA, despite resonances being taken into account. This is most likely because a mass width is implemented in TAUOLA

which smooths out the step function, while the resonances were assumed to have a fixed mass in PROPOSAL. This argument is further supported by the fact that close to energy fractions of 0.2, at the ρ meson resonance, the TAUOLA distributions also have a steep increase, similar to a step function. This is because the ρ meson has a relatively narrow mass width, and therefore results in a steeper increase. Neither the earlier version of PROPOSAL, nor the current version thus simulate hadronic tau decays accurately.

5.1.3 Missing decay modes

Most of the missing decay modes are hadronic decay modes with even higher multiplicity, e.g. $\tau^- \rightarrow \pi^-\pi^-\pi^+\pi^0\nu_\tau$, where the visible energy fraction is larger than for the other decay modes that are implemented in Geant4. These events would increase the average visible energy for cascade-like events among the TAUOLA simulations, which would make the distribution closer to the Geant4 energy distributions, where the energy is overestimated due to the lack of resonances. This is seen by the fact that the discrepancy is greater for an individual hadronic decay mode, e.g. Figure 4.15, than for all cascade-like events in Figure 4.22

Another consequence of the missing decay modes is that the implemented decay modes are overestimated. For example, the muon decay mode fraction has increased from the correct 17% to 19%., i.e. an increase of 2 percentage points or a relative increase of 11%.

5.1.4 Implications for IceCube tau neutrino searches

In total, as seen in Figures 4.22 and 4.23, the visible energy is overestimated for cascade-like events. This means that the light emitted is in reality dimmer than what is predicted by current IceCube simulations. Furthermore, as discussed above, this affects all tau neutrino energies that can be detected at IceCube. The implications of this for tau neutrino appearance searches is that the histogram of tau neutrino events in simulations (such as the one shown in Figure 2.4) is shifted downwards to lower energies. This means that some simulated tau neutrinos with higher reconstructed energy than the currently maximum allowed energy of 56 GeV will be included in the histogram, while some low-energy neutrinos will have a reconstructed energy lower than the minimum allowed energy of 5.6 GeV, and be discarded. From Figure 2.4, we can however predict that in total, there will be fewer events in the histogram. This in turn means that the fit of the tau normalization will increase, to compensate for the decrease in the number of tau neutrino events. Since the current best-fit value of the tau normalization is around 0.75 [4], this will likely shift closer to 1. This means that the results would match better with our current understanding of neutrino oscillations. However, the quantitative shift of the tau normalization due to the improved tau decay simulations remains unknown until full simulations with detector effects are performed.

Since most simulations issues also exist in PROPOSAL, the findings in this thesis also affect IceCube searches for astrophysical tau neutrinos. For example, in Ref. [44], a neural network was trained on simulation data to identify tau neutrinos, and identified seven tau neutrino candidates. However, since the simulations have, through this study,

been found to be incorrect, the neural network has been trained on biased data. The identified tau neutrino events might therefore also be inaccurate.

5.1.5 IceCube simulation improvements

There are several ways of solving the issues with tau decays mentioned above, with benefits and drawbacks for all of them. Three possible solutions are discussed below. The different proposed paths forward are also summarized in Table 5.1.

The first possible solution is to integrate TAUOLA into the IceCube simulation framework. To the author's knowledge, TAUOLA is the most accurate simulation tool for tau decays, as shown in e.g. Section 4.1. Furthermore, TAUOLA does not have any dependencies except for a FORTRAN and C++ compiler (which both are already used in IceCube), which makes it easy to integrate into the rest of the IceCube simulation framework. As a part of the work for this thesis, an integration of TAUOLA into Geant4 has been implemented [45], and integration of tau polarization calculations into the IceCube simulation framework is currently in progress. Adding this integration to any Geant4 application is simple and documented, and once TAUOLA is integrated, the tau leptons are automatically always decayed with TAUOLA, with all decay products immediately being passed back to Geant4 for the rest of the simulation. No integration of TAUOLA into PROPOSAL has been implemented yet.

One potential problem with TAUOLA is that it is a relatively old software and does not seem to be actively maintained. One consequence of this is that some C++ or FORTRAN features used within TAUOLA might be deprecated in the future, resulting in the code not working. Another consequence of the source code not being maintained is that some physical constants, such as the mass of particles, mass widths, and life times are slightly outdated. As an example, the neutrino mass is set to 10 MeV. Though for interactions used in IceCube, with energies on the GeV scale or higher, this erroneous neutrino mass has a negligible effect on the outcome. The improvements in accuracy from using TAUOLA are thus much greater than the errors caused by incorrect physical constants. A third potential problem with TAUOLA integration is that it does not support multi-threading, which can affect the performance of simulations. However, currently the IceCube simulations run on a cluster where simulation jobs are separated into completely separate processes, and each process already runs in a single thread. No effect on the performance is therefore expected for now.

The second proposed solution is to use PYTHIA6 for simulating tau decays. PYTHIA6 is a dependency of GENIE, and no additional dependencies therefore need to be added to the current simulation framework. Furthermore, an implementation of tau decays via PYTHIA6 inside the IceCube simulation framework already exists, making the transition easy [49]. PYTHIA6 does support resonance decays with a mass width, and is in that way superior to Geant4 and PROPOSAL. However, it does not support polarized decays, and since it is not actively maintained by the PYTHIA development team, it will never have this feature. If GENIE at some point switches to using PYTHIA8, there would however be some limited support for polarized decays, as PYTHIA8 supports setting the z component of the polarization vector. One problem with using PYTHIA6 is that the tau lepton would not be passed to PROPOSAL or Geant4 before simulating its decay. This

might be a problem for high-energy ($E \gtrsim 10$ TeV) incoming tau neutrinos, as the tau lepton would travel a non-negligible distance in the ice and lose energy before decaying. How large of an effect this has is however unknown.

The third proposed solution is to implement more sophisticated decay simulations directly into Geant4 and PROPOSAL. This would be the best solution in the long term, as no new dependencies are added, the workflow can remain unchanged, and the propagation simulation of high-energy tau leptons would still remain accurate. However, implementing this feature would be on the time scales of months or years, and be highly dependent on external Geant4 and PROPOSAL developers. Additionally, updating to the newest version of a software is not always simple for large simulations frameworks like the one used in IceCube, and would likely be complicated. Nevertheless, as part of this thesis, both Geant4 and PROPOSAL developers have been contacted and informed of the issues with their current tau decay simulations.

Solution	TAUOLA	PYTHIA6	Update G4, PROPOSAL
Implemented in G4?	Yes	Yes	No
Implemented in PROPOSAL?	No	Yes	No
Fixes resonance?	Yes	Yes	Yes
Fixes polarization?	Yes	No	Yes
New dependencies	TAUOLA	None	None
Tau ice propagation effects	As before	Ignored	As before
Multi-threading	No	Yes	Yes

Table 5.1: Comparisons of the three different proposed solutions to the current tau decay simulations. The proposed solutions are described in detail in the text. Each row addresses an issue and if it is solved by the particular solution. The cell color indicates if it is a positive or negative aspect of the particular solution. Note that "Tau ice propagation effects" means that the tau lepton is allowed to propagate through the ice interact with it, thereby losing energy.

5.2 Future work

The main focus of this study has been on tau neutrinos and not anti-tau neutrinos. In the future, it is therefore necessary to extend this analysis to also account for anti-tau neutrinos. In theory, this is relatively straight-forward, as the only thing that needs to be changed in the current implementation are the $\pm$ and $\mp$ signs in Equations 2.11−2.13.

Since TAUOLA has already been integrated into Geant4, the immediate next step is to use this to simulate tau neutrino interactions in the IceCube simulation framework, using tau decays with TAUOLA and calculating the realistic polarization. Full simulations will be performed, with simulations of the Cherenkov light traveling through the ice, the detector effects, and filtering of the data. From this, it is possible to evaluate how large of an effect the mismodeling of tau decays has on the detected signal. Based on these results, one can then either use the newly simulated samples or add weights on the samples that

were used in the previous simulations to account for the mismodeling. These MC samples can then be used for all upcoming and new tau neutrino appearance searches.

In the long term, it is also important that the Geant4 and PROPOSAL simulations are updated to take resonances and polarization into account, as discussed in the previous section. Another improvement is to integrate the polarization calculation into GENIE directly. Since there already is a polarization vector field that is stored in the GENIE output, it would be relatively easy to extract this value and pass it to Geant4 while running simulations. Furthermore, many of the polarization calculations already rely on features inside GENIE, such as the GRV98LO PDF with Bodek-Yang corrections for DIS polarization, as well as the Berger-Sehgal model for RES polarization. Integrating the polarization calculation into GENIE would therefore be relatively straightforward.

5.3 Summary and conclusions

IceCube is one of the few neutrino detectors that can detect tau neutrinos. When tau neutrinos interact with the ice, a tau lepton is often formed. This tau lepton almost immediately decays to one or more neutrinos, which are not detected, and other decay products that produce Cherenkov light, which are detected and used to reconstruct the energy of the incoming tau neutrino. Accurate simulations of the energy and direction of the visible decay products is therefore crucial to be able to study the incoming tau neutrinos.

In this study, the current status of tau lepton decays within the IceCube simulation framework is investigated. Currently, GENIE is used to simulate neutrino-nucleus interactions, but the tau lepton is not decayed within GENIE. Instead, for low-energy interactions, the tau neutrino is passed to Geant4 to simulate the decay, while for high-energy interactions, the tau lepton is passed to PROPOSAL where the decay is simulated. Three major problems were found with the current decay simulations: the tau polarization (also known as helicity) is not calculated and not accounted for during the decays, hadronic resonances are not simulated, and roughly 13% of the decay modes are not implemented in Geant4. These problems result in a non-negligible mismodeling for 65% of the tau decays.

The current Geant4-based tau decay simulations were compared to tau decay simulations with TAUOLA, a software library for precision tau decay simulations. TAUOLA simulates resonances, rare decay modes, and can also take tau polarization into account. TAUOLA does however not calculate the polarization on its own. To resolve this problem, the formulas for calculating the tau polarization were implemented, with the four-momenta of the tau lepton, tau neutrino, and nucleon as the main inputs. From the implemented calculations, we find that the tau polarization tends to be left-handed, i.e., the spin vector is anti-parallel to the momentum vector, especially for high-energy tau neutrinos.

By evaluating the tau polarization vector for each neutrino-nucleus interaction and passing this to TAUOLA, accurate tau decay simulations could be performed. These "correct" (as far as we know) tau decays were compared to the Geant4 decays. From this, we found that the visible energy (i.e. the energy sum of all non-neutrino decay

products) of the tau is typically larger for the current IceCube tau decays, compared to the "correct" TAUOLA simulations. For IceCube, this means that tau neutrino events are in reality dimmer than what the simulations predicted. The energy discrepancy appears for all tested tau neutrino energies from 5 to 100 GeV, and extrapolations show that the error also exists for all higher energies. Since the mismodeling exists in both Geant4 and PROPOSAL, the energy discrepancy affects both simulations of atmospheric neutrinos used for neutrino oscillation studies and measurements of astrophysical tau neutrinos. There is also a small discrepancy between the simulated direction of the decay products in Geant4 compared to TAUOLA, though this discrepancy is negligible for all energies investigated here.

To resolve the energy discrepancy issue in the current Geant4-based IceCube simulations, software was developed that integrates TAUOLA into Geant4. This makes it such that all tau leptons are decayed using TAUOLA, and the decay products are then passed back to Geant4. This has been integrated into the IceCube simulations used for the next tau neutrino appearance study, including the full polarization vector calculations. How the energy discrepancy and mismodeling affects the reconstructed tau neutrinos, after taking detector effects and ice into account, will be evaluated in the near future. This is done by using the Geant4-TAUOLA integration simulating full tau neutrino samples, from the neutrino-nucleus interaction, to decays, to ice propagation, detector effects, triggers, and more. These results are however beyond the scope of this thesis.

In the future, the goal is to implement more accurate tau decay simulations directly into Geant4 and PROPOSAL, as well as integrating the polarization vector calculations into GENIE. Developers for all of these software libraries have therefore been contacted and informed of the current issues with their simulations.

Chapter 6

Acknowledgements

I would like to thank my supervisors Jason Koskinen, Chad Finley, and Christian Ohm for the guidance and providing feedback on this thesis. I would also like to thank the rest of the IceCube research group at the Niels Bohr Institute for helpful discussions. In particular, I would like to thank Tom Stuttard for helpful discussions and generating IceCube DeepCore simulation samples. I would also like to thank the particle physics group at Stockholm University for providing a place to work at and for fun discussions during lunch and fika. I am also grateful for the many discussions, feedback and help that I have received from various members in the particle physics and IceCube community, including (but not limited to) Alfonso Garcia, Vadim Naumov and Joshua Isaacson. I would also like to thank my opponent Olle Lndberg and my examiner Jonas Strandberg for comments on the thesis and during the defense.

Lastly, I would like to thank the Anders Wall foundation for funding my visits to the Niels Bohr Institute in Copenhagen.

Bibliography

[1] Carlo Giunti and Chung W Kim. *Fundamentals of neutrino physics and astrophysics*. Oxford university press, 2007.

[2] R. L. Workman et al. Review of Particle Physics. *PTEP*, 2022:083C01, 2022. doi: 10.1093/ptep/ptac097.

[3] Etienne Bourbeau. *Measurement of Tau Neutrino Appearance in 8 years of IceCube Data and A Search for Astrophysical Neutrinos from the Local Universe*. Phd thesis, University of Copenhagen, February 2021. Available at https://nbi.ku.dk/english/research/experimental-particle-physics/icecube/group_theses/Bourbeau_thesis_version_soumise.pdf.

[4] M. G. Aartsen et al. Measurement of atmospheric tau neutrino appearance with icecube deepcore. *Physical Review D*, 99(3), February 2019. ISSN 2470-0029. doi: 10.1103/physrevd.99.032007. URL http://dx.doi.org/10.1103/PhysRevD.99.032007.

[5] Markus Ahlers, Klaus Helbing, and Carlos Pérez de los Heros. Probing particle physics with icecube. *The European Physical Journal C*, 78(11):924, 2018.

[6] IceCube Collaboration. Time-integrated neutrino source searches with 10 years of icecube data. *Phys. Rev. Lett.*, 124:051103, Feb 2020. doi: 10.1103/PhysRevLett.124.051103. URL https://link.aps.org/doi/10.1103/PhysRevLett.124.051103.

[7] Sw. Banerjee and A. Lusiani. τ branching fractions, 2022. URL https://pdg.lbl.gov/2023/reviews/rpp2023-rev-tau-branching-fractions.pdf.

[8] Mario Dunsch, Jan Soedingrekso, Alexander Sandrock, Maximilian Meier, Thorben Menne, and Wolfgang Rhode. Recent improvements for the lepton propagator proposal. *Computer Physics Communications*, 242:132–144, September 2019. ISSN 0010-4655. doi: 10.1016/j.cpc.2019.03.021. URL http://dx.doi.org/10.1016/j.cpc.2019.03.021.

[9] C. Amsler, S. Eidelman, A. Masoni, and G. Venanzoni. Spectroscopy of Light Meson Resonances, 2022. URL https://pdg.lbl.gov/2022/reviews/rpp2022-rev-light-mesons-spectroscopy.pdf.

[10] Eliecer Hernández, Juan Nieves, Federico Sánchez, and Joanna E Sobczyk. Tau longitudinal and transverse polarizations from visible kinematics in (anti-) neutrino nucleus scattering. *Physics Letters B*, 829:137046, 2022.

[11] B.K. Bullock, K. Hagiwara, and A.D. Martin. Tau polarization and its correlations as a probe of new physics. *Nuclear Physics B*, 395(3):499–533, 1993. ISSN 0550-3213. doi: https://doi.org/10.1016/0550-3213(93)90045-Q. URL https://www.sciencedirect.com/science/article/pii/055032139390045Q.

[12] K. Hagiwara, K. Mawatari, and H. Yokoya. Tau polarization in tau-neutrino nucleon scattering. *Nuclear Physics B*, 668(1–2):364–384, September 2003. ISSN 0550-3213. doi: 10.1016/s0550-3213(03)00575-3. URL http://dx.doi.org/10.1016/S0550-3213(03)00575-3.

[13] Konstantin S. 'Kuzmin, Vladimir V. Lyubushkin, and Vadim A.' Naumov. Lepton polarization in neutrino–nucleon interactions. *Modern Physics Letters A*, 19(38): 2815–2829, December 2004. ISSN 1793-6632. doi: 10.1142/s0217732304016172. URL http://dx.doi.org/10.1142/S0217732304016172.

[14] Luis Alvarez-Ruso, Costas Andreopoulos, Adi Ashkenazi, Christopher Barry, Steve Dennis, Steve Dytman, Hugh Gallagher, Alfonso Andres Garcia Soto, Steven Gardiner, Walter Giele, Robert Hatcher, Or Hen, Libo Jiang, Igor D. Kakorin, Konstantin S. Kuzmin, Anselmo Meregaglia, Vadim A. Naumov, Afroditi Papadopoulou, Marco Roda, Vladyslav Syrotenko, Júlia Tena-Vidal, Jeremy Wolcott, Natalie Wright, Monireh Kabirnezhad, and Narisoa Vololoniaina. Recent highlights from genie v3. *The European Physical Journal Special Topics*, 230(24):4449–4467, December 2021. ISSN 1951-6401. doi: 10.1140/epjs/s11734-021-00295-7. URL http://dx.doi.org/10.1140/epjs/s11734-021-00295-7.

[15] A. Bodek and J. L. Ritchie. Fermi-motion effects in deep-inelastic lepton scattering from nuclear targets. *Phys. Rev. D*, 23:1070–1091, Mar 1981. doi: 10.1103/PhysRevD.23.1070. URL https://link.aps.org/doi/10.1103/PhysRevD.23.1070.

[16] Ch. Berger and L. M. Sehgal. Lepton mass effects in single pion production by neutrinos. *Physical Review D*, 76(11), December 2007. ISSN 1550-2368. doi: 10.1103/physrevd.76.113004. URL http://dx.doi.org/10.1103/PhysRevD.76.113004.

[17] Dieter Rein and Lalit M Sehgal. Neutrino-excitation of baryon resonances and single pion production. *Annals of Physics*, 133(1):79–153, 1981.

[18] Konstantin S. Kuzmin, Vladimir V. Lyubushkin, and Vadim A. Naumov. Extended rein–sehgal model for tau lepton production. *Nuclear Physics B - Proceedings Supplements*, 139:158–161, February 2005. ISSN 0920-5632. doi: 10.1016/j.nuclphysbps.2004.11.213. URL http://dx.doi.org/10.1016/j.nuclphysbps.2004.11.213.

[19] Arie Bodek, Un Ki Yang, and Yang Xu. Inelastic axial and vector structure functions for lepton-nucleon scattering 2021 update, 2021.

[20] Andy Buckley, James Ferrando, Stephen Lloyd, Karl Nordström, Ben Page, Martin Rüfenacht, Marek Schönherr, and Graeme Watt. Lhapdf6: parton density access in the lhc precision era. *The European Physical Journal C*, 75(3), March 2015. ISSN 1434-6052. doi: 10.1140/epjc/s10052-015-3318-8. URL http://dx.doi.org/10.1140/epjc/s10052-015-3318-8.

[21] Costas Andreopoulos, Christopher Barry, Steve Dytman, Hugh Gallagher, Tomasz Golan, Robert Hatcher, Gabriel Perdue, and Julia Yarba. The GENIE Neutrino Monte Carlo Generator: Physics and User Manual. *arXiv*, 10 2015.

[22] COHERENT Collaboration. Coherent elastic neutrino-nucleus scattering: Terrestrial and astrophysical applications, 2022.

[23] C. Andreopoulos et al. The GENIE Neutrino Monte Carlo Generator. *Nucl. Instrum. Meth. A*, 614:87–104, 2010. doi: 10.1016/j.nima.2009.12.009.

[24] Júlia Tena-Vidal et al. Neutrino-nucleon cross-section model tuning in GENIE v3. *Phys. Rev. D*, 104(7):072009, 2021. doi: 10.1103/PhysRevD.104.072009.

[25] Torbjörn Sjöstrand, Stephen Mrenna, and Peter Skands. PYTHIA 6.4 physics and manual. *Journal of High Energy Physics*, 2006(05):026–026, may 2006. doi: 10.1088/1126-6708/2006/05/026. URL https://doi.org/10.1088%2F1126-6708%2F2006%2F05%2F026.

[26] Rene Brun, Fons Rademakers, Philippe Canal, Axel Naumann, Olivier Couet, Lorenzo Moneta, Vassil Vassilev, Sergey Linev, Danilo Piparo, Gerardo GANIS, Bertrand Bellenot, Enrico Guiraud, Guilherme Amadio, wverkerke, Pere Mato, TimurP, Matevž Tadel, wlav, Enric Tejedor, Jakob Blomer, Andrei Gheata, Stephan Hageboeck, Stefan Roiser, marsupial, Stefan Wunsch, Oksana Shadura, Anirudha Bose, CristinaCristescu, Xavier Valls, and Raphael Isemann. root-project/root: v6.18/02, August 2019. URL https://doi.org/10.5281/zenodo.3895860.

[27] S. Agostinelli, J. Allison, K. Amako, J. Apostolakis, H. Araujo, P. Arce, M. Asai, D. Axen, S. Banerjee, G. Barrand, et al. Geant4—a simulation toolkit. *Nuclear Instruments and Methods in Physics Research Section A: Accelerators, Spectrometers, Detectors and Associated Equipment*, 506(3):250–303, 2003. ISSN 0168-9002. doi: https://doi.org/10.1016/S0168-9002(03)01368-8. URL https://www.sciencedirect.com/science/article/pii/S0168900203013688.

[28] John Allison, Katsuya Amako, JEA Apostolakis, HAAH Araujo, P Arce Dubois, MAAM Asai, GABG Barrand, RACR Capra, SACS Chauvie, RACR Chytracek, et al. Geant4 developments and applications. *IEEE Transactions on nuclear science*, 53(1):270–278, 2006.

[29] J. Allison, K. Amako, J. Apostolakis, P. Arce, M. Asai, T. Aso, E. Bagli, A. Bagulya, S. Banerjee, G. Barrand, et al. Recent developments in Geant4. *Nuclear Instruments and Methods in Physics Research Section A: Accelerators, Spectrometers, Detectors and Associated Equipment*, 835:186–225, 2016. ISSN 0168-9002. doi:

https://doi.org/10.1016/j.nima.2016.06.125. URL https://www.sciencedirect.com/science/article/pii/S0168900216306957.

[30] Jan-Hendrik Koehne, Katharina Frantzen, Martin Schmitz, Tomasz Fuchs, Wolfgang Rhode, Dmitry Chirkin, and J Becker Tjus. Proposal: A tool for propagation of charged leptons. *Computer Physics Communications*, 184(9):2070–2090, 2013. doi: 10.1016/j.cpc.2013.04.001.

[31] M. Chrzaszcz, T. Przedzinski, Z. Was, and J. Zaremba. Tauola of τ lepton decays—framework for hadronic currents, matrix elements and anomalous decays. *Computer Physics Communications*, 232:220–236, 2018. ISSN 0010-4655. doi: https://doi.org/10.1016/j.cpc.2018.05.017. URL https://www.sciencedirect.com/science/article/pii/S0010465518301802.

[32] ATLAS Collaboration. Measurement of τ polarization in $w \to \tau\nu$ decays with the atlas detector in pp collisions at $\sqrt{s} = 7$ TeV. *The European Physical Journal C*, 72(7), July 2012. ISSN 1434-6052. doi: 10.1140/epjc/s10052-012-2062-6. URL http://dx.doi.org/10.1140/epjc/s10052-012-2062-6.

[33] Super-Kamiokande Collaboration. Measurement of the tau neutrino cross section in atmospheric neutrino oscillations with super-kamiokande. *Physical Review D*, 98(5), September 2018. ISSN 2470-0029. doi: 10.1103/physrevd.98.052006. URL http://dx.doi.org/10.1103/PhysRevD.98.052006.

[34] Yoshinari Hayato and Luke Pickering. The neut neutrino interaction simulation program library. *The European Physical Journal Special Topics*, 230(24):4469–4481, 2021.

[35] Torbjörn Sjöstrand, Stephen Mrenna, and Peter Skands. A brief introduction to pythia 8.1. *Computer Physics Communications*, 178(11):852–867, 2008.

[36] Philip Ilten. Tau decays in pythia 8. *Nuclear Physics B - Proceedings Supplements*, 253–255:77–80, August 2014. ISSN 0920-5632. doi: 10.1016/j.nuclphysbps.2014.09.019. URL http://dx.doi.org/10.1016/j.nuclphysbps.2014.09.019.

[37] Charles R. Harris, K. Jarrod Millman, Stéfan J. van der Walt, Ralf Gommers, Pauli Virtanen, David Cournapeau, Eric Wieser, Julian Taylor, Sebastian Berg, Nathaniel J. Smith, Robert Kern, Matti Picus, Stephan Hoyer, Marten H. van Kerkwijk, Matthew Brett, Allan Haldane, Jaime Fernández del Río, Mark Wiebe, Pearu Peterson, Pierre Gérard-Marchant, Kevin Sheppard, Tyler Reddy, Warren Weckesser, Hameer Abbasi, Christoph Gohlke, and Travis E. Oliphant. Array programming with NumPy. *Nature*, 585(7825):357–362, September 2020. doi: 10.1038/s41586-020-2649-2. URL https://doi.org/10.1038/s41586-020-2649-2.

[38] The pandas development team. pandas-dev/pandas: Pandas, February 2020. URL https://doi.org/10.5281/zenodo.3509134.

[39] Wes McKinney. Data Structures for Statistical Computing in Python. In Stéfan van der Walt and Jarrod Millman, editors, *Proceedings of the 9th Python in Science Conference*, pages 56 – 61, 2010. doi: 10.25080/Majora-92bf1922-00a.

[40] Hans Dembinski, Eduardo Rodrigues, and Anatoli Fedynitch. scikit-hep/pyhepmc: v2.1.1, August 2022. URL https://doi.org/10.5281/zenodo.7013498.

[41] Andy Buckley, Philip Ilten, Dmitri Konstantinov, Leif Lönnblad, James Monk, Witold Pokorski, Tomasz Przedzinski, and Andrii Verbytskyi. The hepmc3 event record library for monte carlo event generators. *Computer Physics Communications*, 260:107310, 2021. ISSN 0010-4655. doi: https://doi.org/10.1016/j.cpc.2020.107310. URL https://www.sciencedirect.com/science/article/pii/S0010465520301181.

[42] Henry Schreiner, Jim Pivarski, and Saransh Chopra. vector, 2024. URL https://github.com/scikit-hep/vector.

[43] J. D. Hunter. Matplotlib: A 2d graphics environment. *Computing in Science & Engineering*, 9(3):90–95, 2007. doi: 10.1109/MCSE.2007.55.

[44] IceCube Collaboration. Observation of Seven Astrophysical Tau Neutrino Candidates with IceCube, 2024. URL https://arxiv.org/abs/2403.02516.

[45] Simon Thor. IceCube tau decay improvements, May 2024. URL https://github.com/simonthor/tau-polarization-icecube.

[46] Geant4 Collaboration. Decay - physics reference manual 11.2 documentation, December 2023. URL https://geant4-userdoc.web.cern.ch/UsersGuides/PhysicsReferenceManual/html/decay/decay.html.

[47] IceCube Collaboration PROPOSAL Collaboration. Particledef.cxx, 2024. URL https://github.com/icecube/icetray/blob/oscNext/PROPOSAL/private/PROPOSAL/particle/ParticleDef.cxx.

[48] Alejandro Diaz. Pre-unblinding request update, 2024. Internal slides.

[49] Yitong Liu. τ decays in Genie vs Geant4, April 2024. Presentation.